6-2017

Computational Fluid Dynamic Modeling and Analysis of Small Scale Horizontal Axis Wind Turbines

Madeline Samuell
Union College - Schenectady, NY

Computational Fluid Dynamic Modeling and Analysis of Small Scale Horizontal Axis Wind Turbines

By

Madeline Samuell

****

Submitted in partial fulfillment of the requirements for Honors in the Department of Mechanical Engineering

UNION COLLEGE

June, 2017

Abstract

SAMUELL, MADELINE Computational Fluid Dynamic Modeling of Horizontal Axis Wind Turbines. Department of Mechanical Engineering, June 2017.

ADVISOR: Professor Jeremy Vanderover

As the demand for wind power grows, the technology used to research and further develop wind power must become more sophisticated. Experiments are expensive and require high end test facilities; a commonly used alternative to experimentation are computational fluid dynamic (CFD) models of wind turbines. For this project, Star-CCM+, a CFD software, was used to determine the power generated by small scale horizontal axis wind turbines. The Reynolds-Averaged Navier Stokes (RANS) equations were applied to the models in order to solve for the average flow. Though a variety of different types of simulations were used, the focus was on a rigid body motion model, a dynamic fluid body interaction (DFBI) model and an actuator disk model (ADM). These three simulations were then validated using experimental data published by the National Renewable Energy Lab and various computational studies. It was determined that the best model of the three was the actuator disk model because it most accurately depicted the wake generated by the turbine. However the values calculated for power generated by the turbines in both the actuator disk model and the rigid body motion model varied significantly from the studies that were used to validate them. The dynamic fluid body interaction model was not successful as the rotation could not be induced by the flow.

Table of Contents:

I.	Introduction	1
	a. Benefits of CFD	1
	b. Turbulence Modeling	3
	c. Modeling Geometry	7
II.	Project Overview	8
	a. Determining CFD Software	8
	b. Choice of Models	10
III.	Rigid Body Motion Model	11
	a. Geometry	11
	b. Physics and Mesh Continua	14
	c. Initial Conditions and Motion	18
	d. Results	20
	e. Validation	26
IV.	Dynamic Fluid Body Interaction Model	27
	a. DFBI Motion	28
	b. Results	28
V.	Actuator Disk Model	31
	a. Star-CCM+ Virtual Disk Model	32
	b. Geometry	33
	c. Physics and Mesh Continua	35
	d. Boundary, Initial Conditions and Rotation	35
	e. Results	36
	f. Validation	42
VI.	Turbulence Model Comparison Study	43
VII.	Conclusions and Recommendations	46
VIII.	Future Work	47
IX.	References	50
X.	Appendices	54

Introduction:

As a result of climate change, a fervent search has ensued to find a clean and renewable energy source. Increasingly, wind power has been seen as a potential solution to that search, leading to a rise in the number of wind farms seen across the country and around the world. While large-scale wind power is relatively commonplace, wind power in the private sector, that is residential and small-scale wind turbines, is infrequent.

For this project, computational fluid dynamics (CFD) will be used to model small-scale wind turbines. A variety of computational methods will be explored throughout these analyses, such as Reynolds average Navier-Stokes (RANS), Large-Eddy Simulation (LES), Actuator Disk and Line models (ALM and ADM) and 2D and 3D models, a few of which will be implemented into models.

Benefits of CFD

Computational fluid dynamic analyses are frequently employed in order to examine the flow patterns around wind turbines. One of the most common reasons for this is to learn about the wake created by the wind turbine, which in turn is used to study wind turbine interactions. This is necessary when planning the layout of a wind farm because, if the wind turbines interfere with one another, the wind farm will be less productive. Figure 1 shows results from a CFD simulation of a large wind turbine. It is likely that this model was used to determine whether a wind turbine would be successful in a certain location given conditions like wind speed and geography. Wind turbines are often analyzed using CFD models in order to determine the flow patterns of the wake. The wake generated by the turbine can be seen in figure 1.

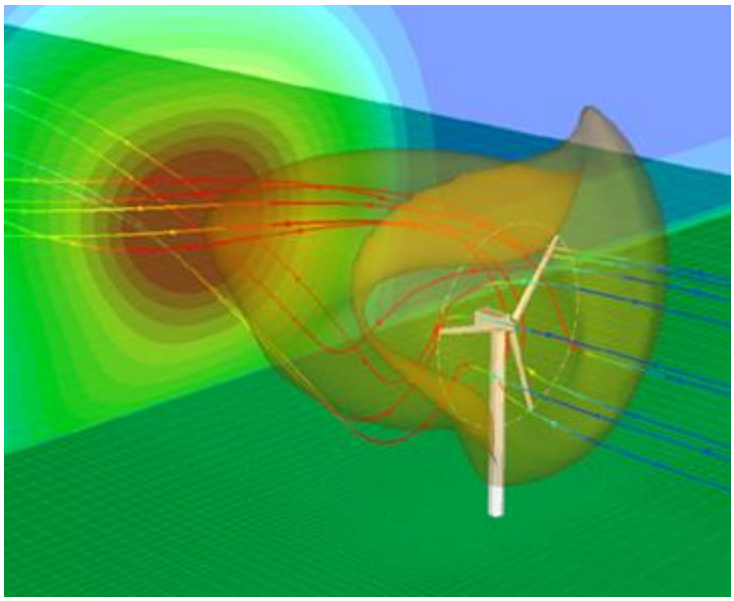

Figure 1: Results of a CFD simulation displaying the wake generated by a wind turbine [1].

It is also possible to gain more accurate energy predictions for a wind turbine by modeling it with CFD. This can be done by examining the average wind speeds a turbine experiences above and below the hub, as well as wind shear and turbulence, and a CFD model can greatly help in this type of study [2].

Computational models are also used when optimizing blade design. There are many different blade designs for turbines, and factors such as the airfoil used along the blade, the chord length of the airfoil, the angle of twist and the tip geometry can all be varied in order to optimize the design and maximize efficiency. Rather than manufacturing and testing a new blade every time a slight change is made, the change can be made to the model and the resulting wake can be analyzed. Therefore, the optimization process is significantly faster and less expensive.

The goal of this project is to use Star CCM+ to model small-scale wind turbines in order to make predictions about the power output of the wind turbine. The power

output of small-scale wind turbines will be very different from large wind turbines and using CFD to predict their power output will determine whether small wind turbines are viable power sources. At the large scale, horizontal axis wind turbines (HAWTs) are the most common because they are the most energy efficient, therefore this study will focus on HAWTS as they are more prominent in the field of wind energy.

Turbulence Modeling

There are a few different methods that can be used to properly model the flow around a wind turbine. The most widely used of these is the Reynolds averaged Navier-Stokes turbulence model (RANS). The Navier-Stokes equations are the governing equations for fluid mechanics and they are used to characterize a flow using different flow parameters, such as pressure, density and velocity. However, the equations are very complicated and can only be solved by making numerous assumptions about the flow to simplify them down to a point where they are able to be solved. Figure 2 shows the incompressible form of the Navier-Stokes equations before they are simplified.

$$\rho\left(\frac{\partial u}{\partial t}+u\frac{\partial u}{\partial x}+v\frac{\partial u}{\partial y}+w\frac{\partial u}{\partial z}\right)=-\frac{\partial p}{\partial x}+\mu\left(\frac{\partial^2 u}{\partial x^2}+\frac{\partial^2 u}{\partial y^2}+\frac{\partial^2 u}{\partial z^2}\right)+\rho g_x$$

$$\rho\left(\frac{\partial v}{\partial t}+u\frac{\partial v}{\partial x}+v\frac{\partial v}{\partial y}+w\frac{\partial v}{\partial z}\right)=-\frac{\partial p}{\partial y}+\mu\left(\frac{\partial^2 v}{\partial x^2}+\frac{\partial^2 v}{\partial y^2}+\frac{\partial^2 v}{\partial z^2}\right)+\rho g_y$$

$$\rho\left(\frac{\partial w}{\partial t}+u\frac{\partial w}{\partial x}+v\frac{\partial w}{\partial y}+w\frac{\partial w}{\partial z}\right)=-\frac{\partial p}{\partial z}+\mu\left(\frac{\partial^2 w}{\partial x^2}+\frac{\partial^2 w}{\partial y^2}+\frac{\partial^2 w}{\partial z^2}\right)+\rho g_z$$

Figure 2: Incompressible form of the Navier-Stokes equations in Cartesian coordinates [3].

Reynolds-average Navier-Stokes is a turbulent flow model, which solves the Navier-Stokes equations by examining the mean flow. Therefore, the sets of equations that are used are time-averaged. This is a very common method used for computation fluid modeling and it is frequently applied to wind turbine models because it yields fairly accurate results within a relatively short computation time.

Different RANS turbulence models can be used depending on the system that is being modeled, the most common of which are k-epsilon, k-omega and spalart-allmaras. These three models are all eddy viscosity models, which use the Reynolds-averaged Navier-Stokes and turbulent viscosity to model the Reynolds stress tensor as a function of the average flow. The k-epsilon and k-omega models are two-equation models, while spalart-allmaras uses only one equation.

Spalart-allmaras model is most suited for cases in which the boundary layer remains attached to the geometry and separation occurs only mildly, such as an airplane wing. It should not be used to model situations where complex recirculation occurs. While this model is more frequently used when modeling airfoils and other simpler geometry, it still is frequently used to model full, rotating wind turbines [10].

The k-epsilon and k-omega models are very similar. They are both better suited than Spalart-Allmaras to simulate recirculating flow, but there are slight differences between the two. A different transport turbulence variable is used for each model and k-omega is typically favored by the aerospace industry and is sometimes used as an alternative to the Spalart-Allmaras model.

Another form of RANS turbulence model available is the Reynolds Stress Transport model. Unlike the other turbulence models, this is not an eddy viscosity model;

it solves for all components of the Reynolds stress tensor, rather than focusing on viscosity like the eddy viscosity models. It is best suited for situations when the flow is very anisotropic, which means that it varies greatly depending on direction. Anisotropy is not a characteristic of flow around a wind turbine, therefore it was determined that this model was not well suited for this application.

Detached eddy simulation (DES) is often used for situations when the unsteadiness in the flow is "imposed or inherent," such as when the boundary conditions are changing significantly with time or there is massively separated flow [11].

Another common method that arose more recently than RANS is Large-Eddy Simulation, or LES. This method differs from RANS in that it removes the smaller aspects of the flow in order to model the large turbulent eddies, thus capturing the larger structures of the flow more accurately. Therefore, rather than averaging the flow, it filters out the small-scale information in the flow, which simplifies the model so that the large aspects of the flow can be modeled directly. While it has been acknowledged that this method typically yields more accurate results than the RANS turbulence model, it requires far more computational time, and is not always a viable option. This length of time is greater because the model is directly solving for the larger aspects of the flow rather than just averaging the flow, like RANS, and directly solving for the large aspect of the flow requires a fine grid. The finer the grid used in a CFD model, the longer the computation time [4]. A paper, which was written about a study in which CFD was used to model the dispersion of pollutants in a city, stated that LES did a much better job at capturing the turbulent mixing of the airflow than RANS. The author argued that LES should be used in situations when the development of the flow field is heavily dependent

on small-scale eddies [5]. Therefore, the tradeoffs must be thoroughly considered, because there are cases where LES will be a much more appropriate model than RANS. Figure 3 shows a comparison between experimental measurements of a flow and the RANS and LES models of the flow.

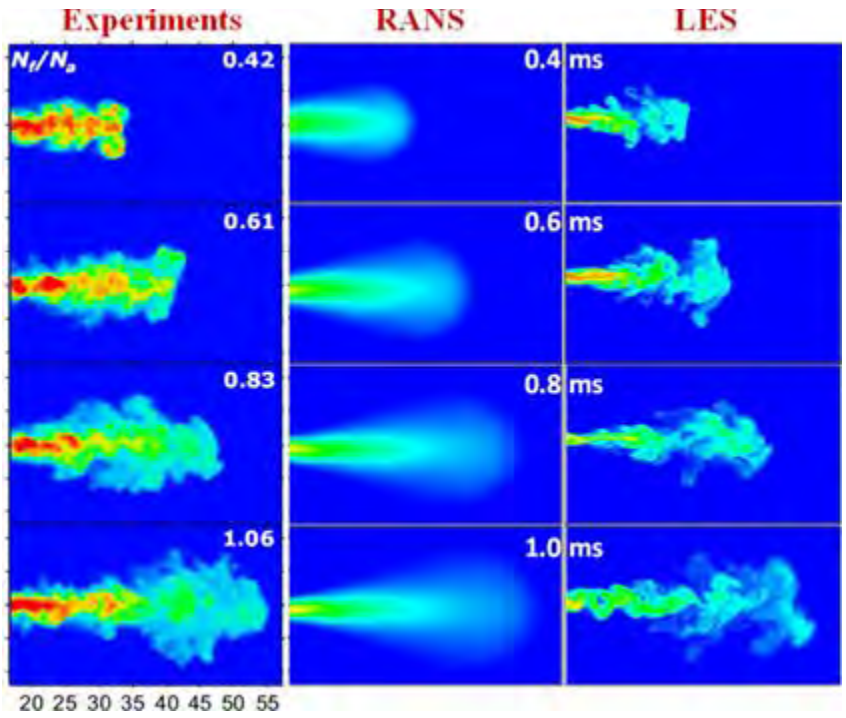

Figure 3: Comparison between experimental results and RANS and LES models [6].

Recently a large amount of literature has been published about models that attempt to combine these two methods. A dissertation entitled “Advanced CFD Methods for Wind Turbine Analysis” uses a hybrid of the two, called HRLES. The motive behind this model is that employs the LES model with a RANS code, to capture the accuracy of LES and the efficiency of RANS [7]. In addition to HRLES, DES, or detached eddy simulation, is another hybrid of LES and RANS that is being used more and more frequently. DES is advantageous because it uses a RANS approach to analyze the

boundary layers and in the separated regions it uses the LES approach. This method cuts down on computation time compared to a complete LES model because it only applies the LES model to the regions where LES is advantageous, for the other regions RANS is used [11].

Modeling Geometry

There have also been significant amounts of research conducted into the way the actual model of the wind turbine should be constructed. In a study conducted by the National Renewable Energy Laboratory (NREL), a wind turbine was modeled in a variety of simple and more complex forms to see whether accurate results could still be obtained from a model that did not contain some of the more complicated aspects of the turbine geometry, such as the tower and the nacelle. Studies were carried out in which the entire turbine was modeled, while other studies used models that incorporated only the blades. In addition to the two extreme cases, some models left out only a few of the more extraneous parts of the turbine [7]. It was determined that the results did not significantly differ, but the computation time decreased significantly for the simpler models. Thus it is usually beneficial to simplify the models in order to minimize computational power.

There are two very simplified models that can be used for a horizontal axis wind turbine and both methods have an extensive amount of literature published about them. They are actuator line model (ALM) and actuator disk model (ADM). ALM models the blades of the turbine as simple lines, while ADM models the blades of the turbine as a porous rotating disk. ADM can accurately model far wakes caused by the turbine and ALM is typically used to model the vortices in the wake caused by the tips of the blades.

Though these models cannot capture all of the details of the flow, they can act as rough estimators for the flow, and produce useful results [12].

Research has also been done to compare the difference between two dimensional and three dimensional models. In general, 3D models yield similar results to 2D models, but require far more computational power; therefore they may not provide an advantage [8]. Therefore, it can be concluded that while the more complicated models will yield the most accurate results, simplifying the models down saves computational power and the accuracy does not greatly suffer.

Project Overview:

The purpose of this research is to model small-scale horizontal axis wind turbine using a variety of methods. The models will then be analyzed to study the wake characteristics and the power generated by the turbines will be calculated based on the values obtained from the simulation. Finally, the models created will be validated using experimental results and results published by research based on other computational fluid dynamic models.

Determining CFD Software

The first step of this research was to determine the CFD program that would be used for the analysis. The options were OpenFOAM or Star-CCM+. OpenFOAM stands for Open-source Field Operation And Manipulation. Open source means that a license is not required to download and use the program; it's completely free. Star-CCM+ does require a license and its relatively costly, therefore it is typically only used by companies,

universities and research institutes. OpenFOAM on the other hand is easily accessible to the general public. This gives OpenFOAM an advantage for the purposes of this project because there is a large amount of online tutorials and message boards discussing the different turbulence models and how to apply them in a simulation. The disadvantage is the program runs through a computer's terminal and users typically choose to download a GUI (graphical user interface) to make carrying out the analysis much simpler. However, the most common GUIs, such as HELYX-OS and enGrid, were not available for download for a Macbook or were not compatible with a Macbook, which was the computer being used to carry out this research. OpenFOAM was initially the favored option, so in order to make OpenFOAM work on a Mac, a virtual machine was downloaded so that a Linux system could be used rather than a Mac OS X, because OpenFOAM is far more compatible with Linux. However, the system was very slow, and would not have been able to handle the computational power required to run the CFD programs, therefore it was decided that OpenFOAM was not a viable option for this project.

Once it was determined that Star-CCM+ was the most practical CFD program for this research, it was necessary to determine the various turbulence models available within the program and how to set them up for a simulation. RANS, LES and DES simulations can all be modeled in Star-CCM+ and the common eddy viscosity turbulence models that were listed previously are also available.

Choice of Models

While it is worth exploring the difference between results yielded by RANS, LES and DES, RANS turbulence modeling is the most compatible with the goals of this research because it requires the least amount of computation time, but still yields accurate results. This is desirable for the purposes of this project because low computation time means that many more models can be tested and run, thus models using all three of the eddy viscosity turbulence models can be tested, different geometries can be adjusted, and inputs, such as the free stream velocity, can also be varied. In addition, LES provides the greatest advantage over other methods because of its accurate modeling of the flow behind a wind turbine, as shown in figure 3. The goal of this project is to calculate power values for wind turbines and the flow is a secondary aspect of the simulations that will be analyzed. The complexity of a LES model will be superfluous because a RANS model and a LES have the same capability to determine power generated. Therefore, RANS models will be the focus of this project.

All three eddy viscosity models are commonly used by researchers in CFD studies, therefore a comparison study will be conducted. Three identical models will be run, and each will use a different turbulence model, any difference in results will be a direct effect of the turbulence model that was used.

Three different types of simulations will also be explored throughout this research; a rigid body motion model, a dynamic fluid body interaction model and an actuator disk model. A rigid body motion model was selected because it is a standard way of modeling a wind turbine in which a CAD model of a turbine is meshed and a rotation rate is set. This type of simulation can be time consuming due to the complicated mesh

that is employed. A dynamic fluid body interaction (DFBI) simulation was also carried out because the same geometry and mesh that were used for the rigid body model can also be applied to the DFBI model. The difference is, rather than setting a rotation rate, the rotation is driven by the free stream velocity. Everything between the two simulations is the same, other than the method used to carry out the rotation, therefore, a comparison between these two studies can be made.

The third type of simulation was an actuator disk model (ADM). These models have been proven to be accurate, yet they do not require much computation time, and the set-up is not complicated. In addition, no specific CAD model is needed for the simulation, so the data for any turbine can be entered into the model. Therefore, this study can be validated using any published and experimental data because any turbine can be modeled. An actuator disk model was chosen over an actuator line model because the ALM is used to study the vortices created by the tips of the blades and ADM is used more often to study the wake. For this research, the wake was deemed more important, thus the ADM method was selected.

Rigid Body Motion Model:

The first type of wind turbine model that was simulated for this research was a rigid body motion model.

Geometry

A CAD model of a small horizontal axis wind turbine was downloaded from the free CAD sharing database GrabCAD. The turbine is shown in figure 4.

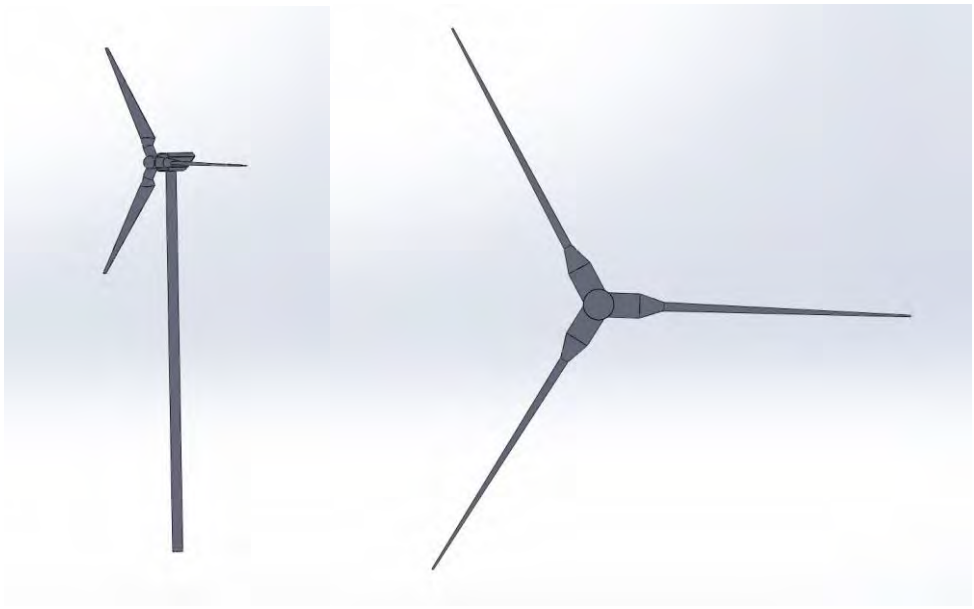

Figure 4: CAD model of a horizontal axis wind turbine that was used for both the rigid body motion model and the dynamic fluid body interaction model. The tower and nacelle are both pictured on the left, but they were removed from the model when imported into Star-CCM+. The model that was meshed is shown on the right [13].

The model that was selected has a mass of 17.15kg, with a blade length of 1.024m. In SolidWorks, the material was defined to be aluminum. The dimensions and mass of the turbine are not directly entered into Star-CCM+ with when the part is imported, however they can be set within the program.

In order to simulate flow around or through an object in Star-CCM+, a part must be created around the entire object. Typically this part is a block or a cylinder, and it defines the background region for the system. The size of the part varied depending on the size of the turbine being tested, but a large amount of space was left both in front of and behind the turbine so that the flow had enough time to develop before it reached the turbine and the wake could fully extend behind it. Boundary conditions then had to be

assigned to the background region. The front was set as a velocity inlet, the back was a pressure outlet and, for a cylindrical region, the entire side was set as a slip wall. This boundary condition is important because if the wall was set as no-slip, the velocity of the flow at the wall would be zero, meaning the flow would not only be affected by the rotating turbine, it would also be heavily influenced by the wall. It is necessary to have these sides on the region in order to constrain the flow from leaving the background region out of the sides. Setting the boundary as a slip wall ensures that the direction of the flow is controlled but it behaves as if the wall is not there. For a block, the top and bottom surfaces were set to slip walls and the left and right sides were set as symmetry planes so that the normal velocities to the boundary are zero, meaning the flow across the boundary is zero [11]. Figure 5 shows an example of a turbine in a rectangular domain, the side is hidden so the turbine is visible.

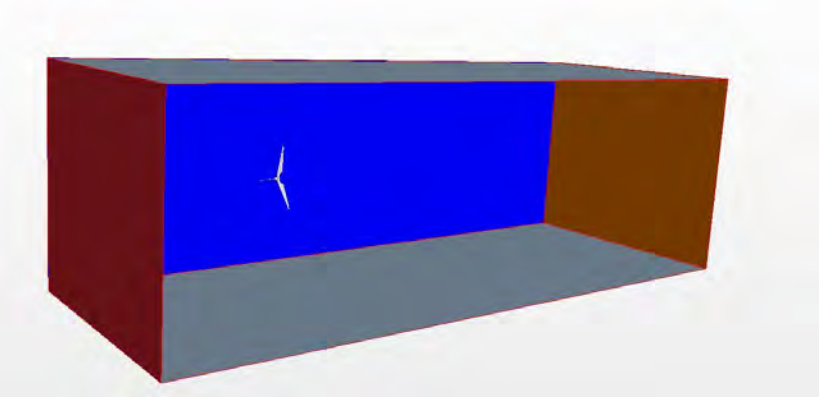

Figure 5: Rectangular domain, with one of the side walls hidden to show the horizontal axis wind turbine inside the region.

A cylindrical domain was primarily used throughout this research; however, the block was shown above because it gives a clearer depiction of the domain and the turbine.

A cylinder was preferred because the number of boundary conditions that have to be applied is limited, which simplifies the simulation [14].

A second part then had to be created around the turbine. This was a small disk that was only slightly larger than the turbine and it was defined as an overset mesh.

Physics and Mesh Continua

Once the geometry is created, the physics and mesh continua were set up. For the three simulations that were tested, the physics continua varied only slightly. This was a three-dimensional simulation because the turbine that was meshed was 3D and it was determined that it should not be simplified down to a two-dimensional model. This study was conducted with steady, turbulent flow, which was defined as incompressible because there are no changes in density as the air travels through the turbine. The RANS turbulence and the spalart-allmaras turbulence model were applied. The spalart-allmaras turbulence model was initially used for all three types of simulations. Comparisons between results yielded by the different turbulence models will be discussed in later sections.

The most complicated part of this study was determining the best mesh to use. The turbine had to be meshed separately from the background region because the turbine was rotating. To achieve this, an overset mesh was used. Overset meshes are applied to CFD studies with complicated geometries or moving parts because it creates a separate, overlapping portion of the mesh (the overset) that meshes only specific bodies in the flow field [4]. Therefore, in this rigid body motion simulation, an overset mesh was created for the turbine that was finer than the mesh used on the background domain. The turbine mesh

overlapped with the background mesh, but was separate, thus the turbine could rotate without the entire background domain having to rotate.

A surface mesh and volume mesh were required for this simulation and to simplify the model, the same meshers were used for both the background and overset mesh. There are two surface meshes available on Star-CCM+, surface remesher and surface wrapper. A surface remesher was selected over the surface wrapper because the surface wrapper is used for geometries with surfaces that intersect or contain gaps or holes, but a surface remesher is typically used for closed geometries [15]. The turbine geometry is closed, indicating a surface remesher is sufficient.

The volume meshers available are polyhedral, tetrahedral, trimmed, thin mesh, and advancing layer mesher. A trimmed mesh was used because it typically produces more accurate results than tetrahedral meshes (about the same level of accuracy as a polyhedral mesh) and it produces a decent quality of mesh, regardless of the surface quality of the original CAD model, making it more reliable [15].

The background mesh, which was applied to the cylindrical region created around the turbine, had a base size of 0.25m. Given that the length of one of the blades of the turbine used in this simulation was 1.024m, this is a relatively large mesh size. However, since there is not a huge amount of change happening in the background, this size is sufficient. If the base size was decreased further, the computation time would have been significantly higher. Two volumetric controls were also applied to the background mesh. A volumetric control is a region of the mesh where more accuracy is needed so the mesh is altered slightly without having to make a whole new mesh. For the background region, the controls were the air inlet and the overlap between the overset mesh and the turbine.

The same meshers were used for both volumetric controls, and for the air inlet, the size of the mesh was kept the same. However, the size of the overlap mesh was reduced from the original base size by 75%, to 0.0625m. This ensured that the region where the background mesh and the overset mesh overlapped was captured in great detail. Figure 6 shows the cylindrical background region after it was meshed.

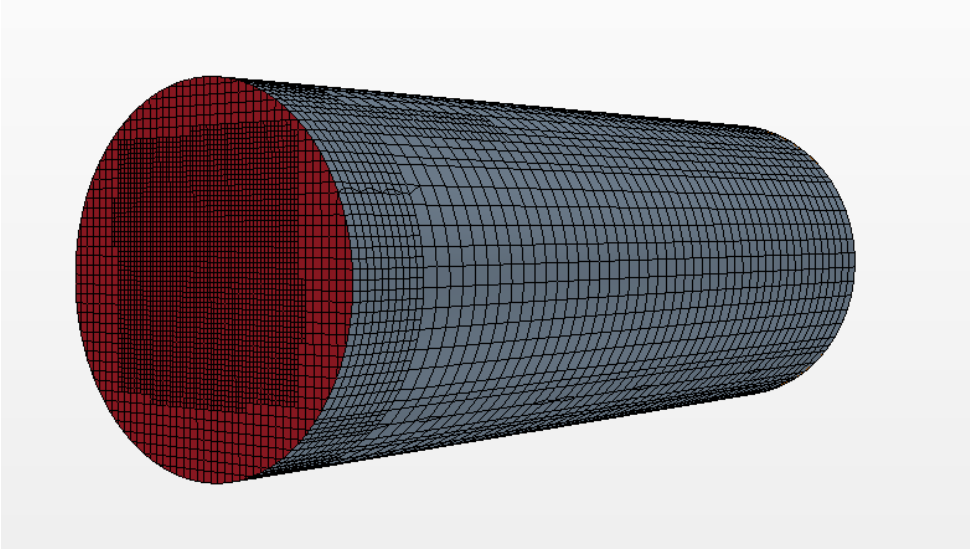

Figure 6: The cylindrical background region with the mesh applied. A refined mesh is shown in the center of the inlet at the end of the cylinder where one of the volumetric controls is located.

The overset mesh was applied to the turbine and the small disk created around the turbine. The surface remesher and trimmed mesh were again applied to this region, but the base size was set to 0.05m, which is much smaller than the base size of the background region. The small size is necessary in this region in order to more accurately capture the complex characteristics of the flow close to the turbine. The only volumetric control for this part of the mesh was the disk around the turbine, named the rotating region, and the size was set to 50% of the base size, meaning it had a size of 0.025m.

Initially, issues were encountered due to setting too large a base size for the mesh. This created holes in the surface of the turbine, as shown by figure 7. It was determined that refining the mesh size further by decreasing the size solved these issues. Figure 8 shows the improved mesh that used a smaller base size of 0.05m.

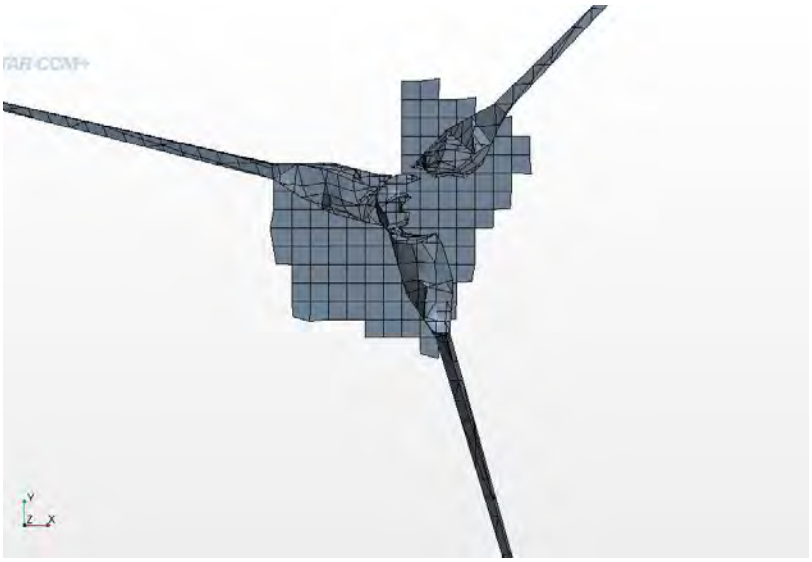

Figure 7: A close up view of an early mesh of the wind turbine. The base size was too large, which lead to holes in the hub of the wind turbine. By decreasing the size of the mesh, this issue was corrected.

Figure 8: Meshed wind turbine with a base size of 0.05m. The turbine has no holes, indicating the mesh is sufficient.

Initial Conditions and Motion

The next step to setting up a simulation was to set the initial conditions for the model. The boundary conditions, which were previously set, are listed below in table 1.

Table 1: Boundary conditions applied to the model

Boundary	**Condition**
Background: Front	Velocity Inlet
Background: Back	Pressure Outlet

Background: Side	Slip Wall
Turbine: Cylinder	Overset Mesh
Turbine: Faces	No-Slip Wall

The faces of the turbine were set as a wall, but unlike the sides of the background region, it was a no-slip wall. This is because there would be friction between the fluid and the surface of the turbine, causing the flow at the surface of the turbine to slow down. Therefore slip does not occur at this boundary.

For the velocity inlet, a velocity of 7.0 m/s along the z-axis was set, which is about 15 mph, a typical wind velocity at low altitudes. It is used for many computational and experimental studies as the lowest velocity tested [10]. The initial free stream velocity was also set to 7.0 m/s in the direction of the z-axis. It was important to make sure these two velocities were set to the same value.

The final aspect to setting up this simulation was to set a rotation for the turbine. Rotation rates in actual turbines is based on the wind speed. However, for most computational studies, the turbine is simulated in steady state conditions and a rotation rate is set based on experimental values and a steady wind speed [14]. The free stream velocity is varied from study to study, which varies the torque of the turbine and, consequently power generated by the turbine, but the rotation rate is held constant. For the studies conducted for this research, the rotation rate was held at 72 RPM, based on the Phase VI wind turbine experiment conducted by the National Renewable Energy Lab (NREL) [16]. This study, the results of which were published in 2001, is frequently used

as for validating results obtained by computational fluid dynamic studies. In the NREL study, extensive tests were conducted to find power produced by a wind turbine operating with a range of inlet velocities. The turbine tested had two blades that used the S809 airfoil. The tests were conducted in the NASA Ames Research Center wind tunnel; the dimensions of the wind tunnel are 40ft X 80ft [16].

To set this rotation rate, a rotating reference frame was created with the origin at [-0.644, 1.737, 2.341] m, the center of the turbine. The rotation was set at 72 RPM and the rotating reference frame was applied only to the turbine, not the background region.

Results

Once everything was set up, the study was conducted. A number of different scenes were created in order to view the behavior of the flow. Figure 9 shows the side profile of the background region. A plane was created through the center of the turbine to capture the flow down the middle of the field and determine the changes in velocity.

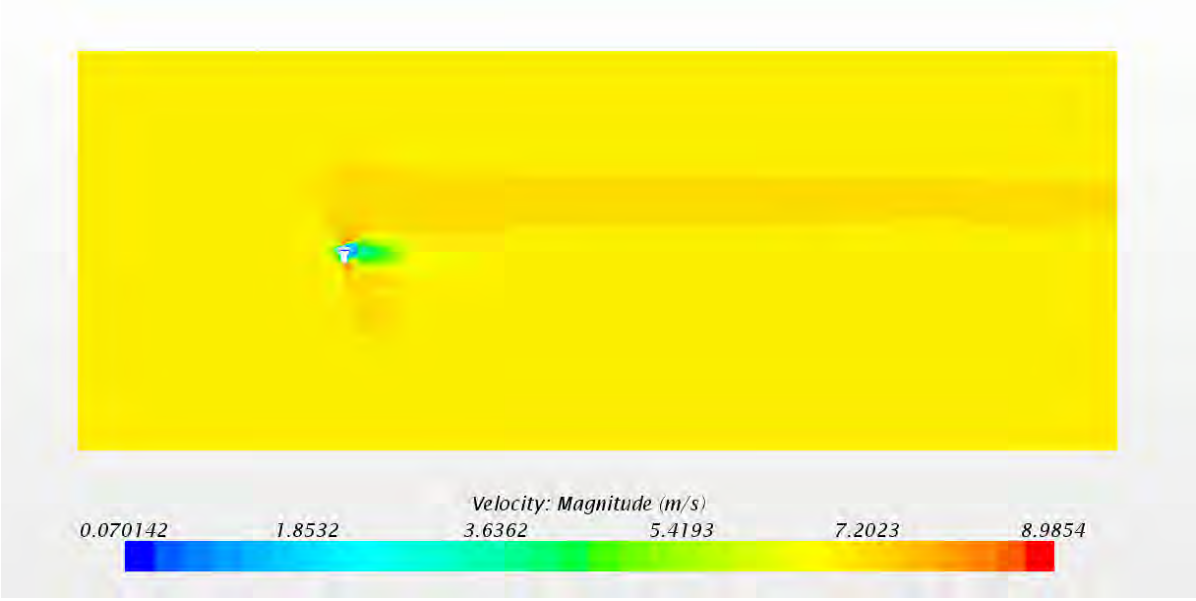

Figure 9: Velocity magnitude in the background region. The inlet is on the right side of the image, so the flow travels from left to right. The hub of the turbine is located where the color change occurs.

The turbine blades are not visible in this image because they lie in different planes, however their effect can still be seen in the image. The velocity enters at 7.0 m/s, as defined by the boundary and initial conditions. A patch of lighter yellow can be seen directly in front of the turbine, this is due to a stagnation point caused by the air hitting the turbine, therefore the air slows down. Darker yellow can be seen above and below the turbine, indicating that the air that is forced around the turbine speeds up, and a portion of this dark yellow above the turbine extends much farther behind the turbine than the rest of the wake. It is unclear why this section of the flow is faster than the rest, however, given the shade of the color, it is estimated to be between 7.3m/s and 8m/s, which is not significantly higher than the surrounding flow. The green and blue directly on the back of the turbine indicates that the air behind the turbine slows down, which is expected.

A plane was constructed that showed the blade in the flow, and the results showed that, though the velocity and the pressure decrease directly behind the hub of the turbine, there is a region of higher velocity and pressure behind the blades. This can be seen in figure 10. This non-uniform region could be due to recirculating flow behind the blades.

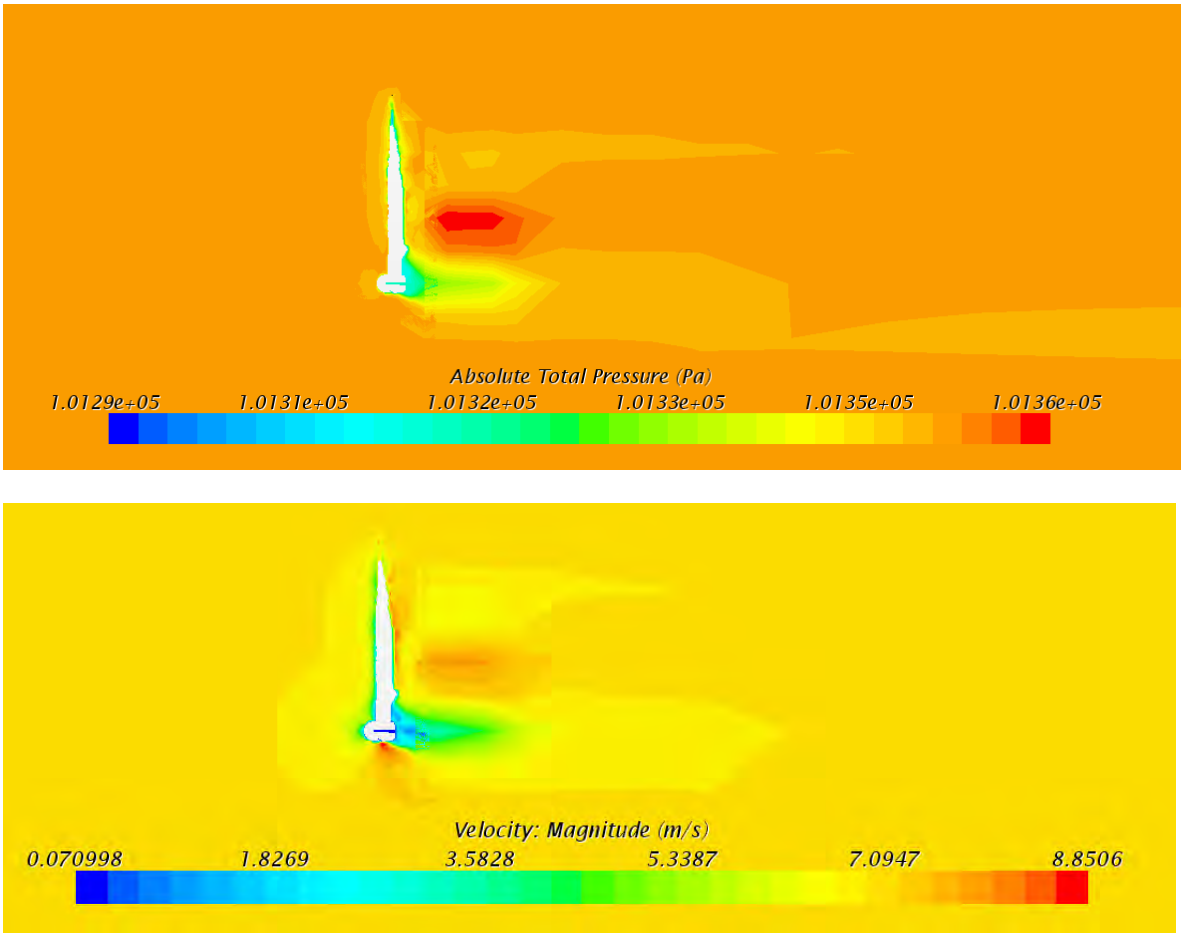

Figure 10: [Top] Pressure contour for the rigid body motion simulation that indicates a region of low pressure behind the turbine hub, but a high-pressure region behind the blade. [Bottom] Velocity contour for the rigid body simulation with regions of high and low velocity in the same high and low pressure regions.

The velocity of the flow around the turbine is shown in figure 11.

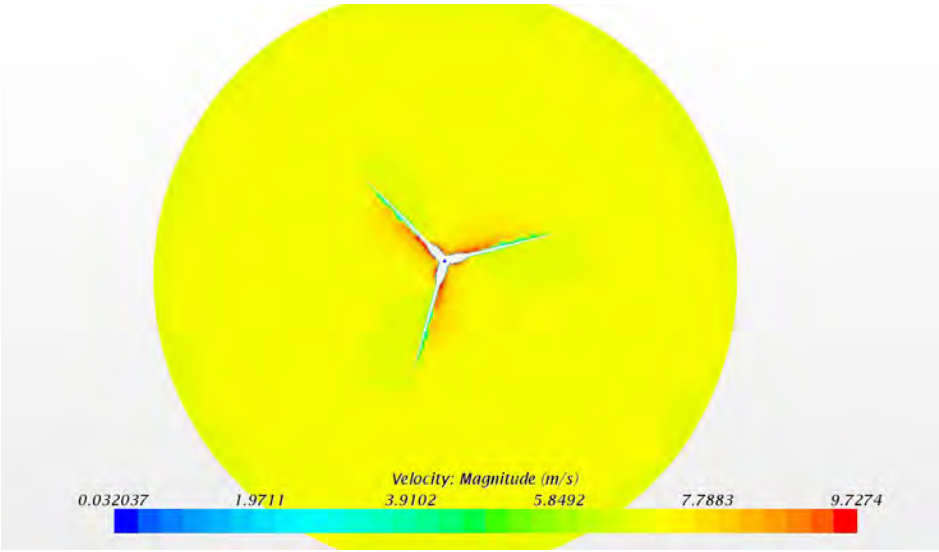

Figure 11: Velocity of the flow around the turbine in the rigid body motion simulation. The turbine is rotating clockwise, and the faster air is shown on the left sides of the blades.

The air is traveling faster on the left side of the blade than on the right because the turbine is spinning clockwise and the faster air on the left side causes a lift force that results in the rotation of the turbine. This is similar to an airplane wing, where the flow under the wing is faster than the flow over the top, creating a lift force that acts upwards on the airplane.

The corresponding pressure contour is shown in figure 12.

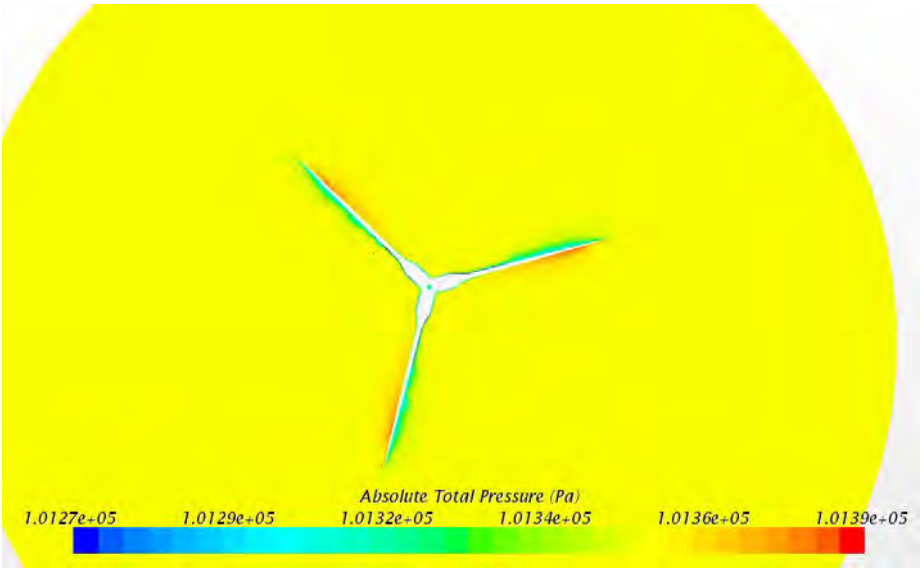

Figure 12: The higher pressure is shown on the right side of the blades.

The high-pressure region occurs on the right side of the blade because the turbine is spinning clockwise, so the right side of the blade is what pushes through the flow, causing an increase in pressure on that surface.

The pressure on the front and back faces of the turbine are shown in figure 13. As expected, the pressure is greater on the front surfaces of the turbine than on the back surfaces of the turbine because the flow stagnates at the front, which increases the pressure.

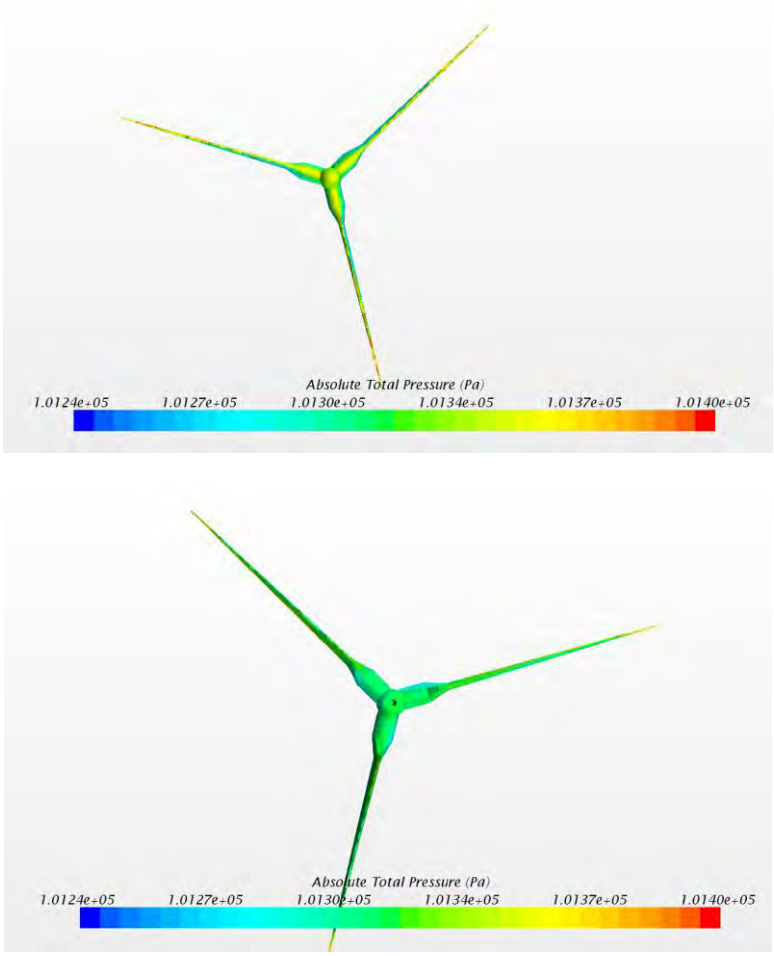

Figure 13: The pressure on the [top] front of the turbine and the [bottom] back of the turbine in the rigid body motion simulation.

The goal of this research was to estimate the power generated by the turbines based on values determined through computational modeling. The long way of determining the power generated by the turbine is to integrate the pressure over the blade to find force, then use the force and the radius of the blades to find torque. Finally, the dot product of torque and angular velocity is taken to calculate power generated [10].

On Star-CCM+ the torque of the turbine can be determined directly by creating a moment report for the turbine and ensuring that the axis origin is located at the origin of

the turbine. The power can then be calculated directly using the value for torque found by the report. The torque was determined to be 2.86 Nm and the angular velocity was 72 RPM, or 7.54 m/s. The equation used to calculate power is shown below.

$$P = \ T\omega = (2.86\ Nm)(72\ RPM) = (2.86\ NM)\left(7.54\frac{rad}{s}\right) = 21.55\ W$$

(1)

The power generated by this turbine was calculated to be 21.55 W.

Validation

The estimated power generated by this turbine was then compared to a turbine that was analyzed in a 2012 study conducted by the University of Western Ontario, which had three blades and a diameter of 2.2 m, as compared to the turbine in this study, which had the same number of blades and a diameter of 2.05 m. The University of Western Ontario study determined that the turbine generated 470W at 9.0 m/s, which is significantly higher than the power determined through CFD. In the University of Western Ontario study, the power output was determined experimentally in a wind tunnel and based on blade element momentum theory calculations. In the experimental setup, the rotation rates that were tested varied from about 500 RPM to 1200 RPM and all the power output values were between 300 W and 1500 W. The BEM theory values were more similar to the CFD results because the rotor speed was tested as low as 85 RPM. At a free stream velocity of 7.0 m/s and a rotor speed of 150 RPM, the power output was about 100 W [17]. While these values are still different from the ones determined using

CFD, they are much closer than the experimental values. Therefore, the values determined in this study are lower than standard published values, but they are not outside the realm of possibility.

Dynamic Fluid Body Interaction Model:

The next study conducted used dynamic fluid body interaction, rather than rigid body rotation and a rotating reference frame. This type of simulation, sometimes called fluid-structure interactions (FSI), differs because the rotation rate is not set within the simulation. Instead, the angular velocity is determined by the wind speed.

In typical simulations, the rotation rate and free stream velocity are independently entered into the program. They need to be adjusted until they are related (i.e. the rotation rate must be reasonable for the wind speed). However, in a dynamic fluid body interaction model the turbine rotation is dependent on the wind speed because the turbine will only rotate once the flow provides enough energy to drive it [14].

The geometry, mesh, boundary conditions and initial conditions used for this study were exactly the same as in the rigid body motion study. The only differences were the way the motion was defined and that the simulation was unsteady. The simulation had to be unsteady because the turbine would initially not be moving, but would eventually reach a constant rate of rotation after the fluid had been flowing past the turbine for a duration of time.

DFBI Motion

In a fluid-structure interaction simulation, the rotation of the turbine is not predetermined, it is a result of the wind speed. Free motion was applied to the turbine, but all motion was restricted except for rotation around the z-axis, which was the axis that ran through the center of the turbine. The center of mass was defined as the origin of the turbine, [-0.673, 1.691. 2.324] m. A moment of inertia also had to be calculated for the turbine. To simplify the calculation, the turbine was assumed to behave like a disk, and the following equations for moment of inertia of a disk were used.

$$I_x = I_y = \left(\frac{1}{4}\right) mr^2 = \left(\frac{1}{4}\right)(17.15\ kg)(1.025\ m)^2 = 4.50\ kgm^2 \quad (2)$$

$$I_z = \left(\frac{1}{2}\right) mr^2 = \left(\frac{1}{2}\right)(17.15\ kg)(1.025\ m)^2 = 9.009\ kgm^2 \quad (3)$$

Therefore the moment of inertia in each direction is [4.5, 4.5, 9.009] kg/m^2.

As in the rigid body motion simulation, the background region was held stationary.

Results

Unfortunately, the results of this simulation were inconclusive, as the turbine did not appear to rotate. Initially the study was run with a velocity of 7.0 m/s, which yielded no rotation. In an attempt to increase the energy input to the turbine, the velocity was raised to 20.0 m/s, however there was still no motion. This was not unexpected, as these

types of simulations are typically more complex than ones where rotation is set. Figure 14 shows a velocity contour of the turbine plane.

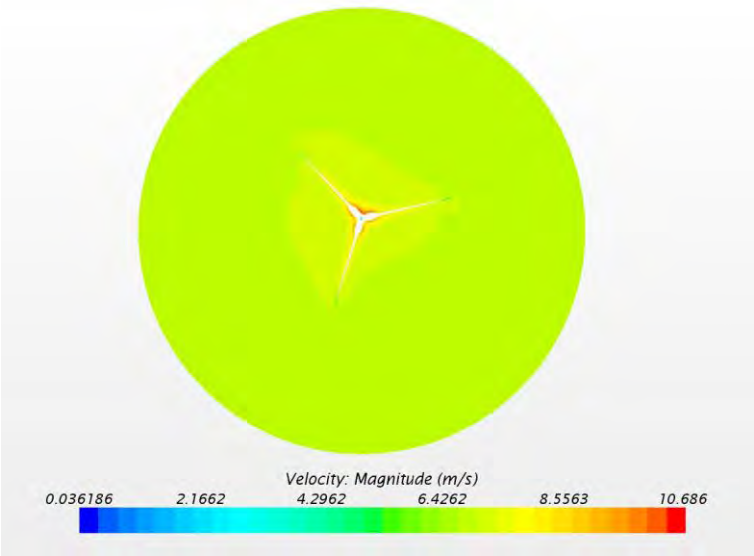

Figure 14: Velocity contour of the turbine plane from the DFBI study with a free stream velocity of 7.0 m/s.

It is clear from this velocity contour that there is no rotation because the flow around the turbine is very uniform and only slight disrupted. Had there been rotation, the contour would resemble the ones from the rigid body rotation study in figure 11. The velocity contour from the study with a 20.0 m/s velocity is identical, and can be seen in appendix 2. The velocity wake is shown in figure 15.

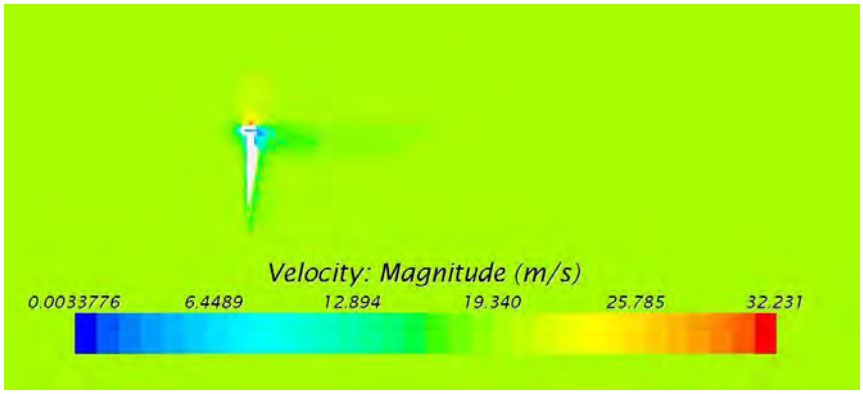

Figure 15: Velocity of the wake of the turbine from the DFBI study, with a free stream velocity of 20.0 m/s.

As shown in the figure above, the flow is only slightly disrupted by the turbine, and the wake is nearly nonexistent. This also indicates that the turbine was not rotating because the wake in this case should be larger and should resemble the wakes shown in the rigid body motion study.

The final step of each study is to calculate the power generated by the wind turbine based on values obtained from the CFD models. For the 7.0 m/s velocity, the torque of the turbine should be the same, or similar to the torque found in the rigid body motion study because all of the conditions were the same except for the method of defining the motion. However, the torque was determined to be 0.058 Nm, compared to 2.86 Nm found in the RBM study. Moreover, there was no measured angular velocity. Therefore the power cannot be calculated for this study and it cannot be validated.

This type of simulation may seem more accurate because it behaves much more like an actual turbine, however there is not a lot of research published regarding wind turbine simulations that utilize this motion. This is because it is an inherently more

complex model and the models where the rotation rate is set tend to be accurate enough that these more complex studies are unnecessary.

Actuator Disk Model:

The final study that was conducted used the actuator disk model, which simplifies the geometry of the turbine by modeling it as a porous disk. The advantage of this model is that meshing required for this turbine is significantly easier because the geometry is a cylindrical disk rather than a turbine, therefore it eliminates the complex meshing that was required in the previous two models. This model was selected over an actuator line model because it typically models the wake more accurately than the actuator line model, while ALM models the vortices created by the tips of the blades [4]. Since the vortices created by the tips were not analyzed in the rigid body motion study or the DFBI study, it was determined that using ADM to analyze the wake would be more beneficial than using ALM. As previously mentioned, CFD studies are frequently validated using NREL results from an experiment conducted in a wind tunnel using the Phase IV turbine. The previous two models could not be validated using this study because a CAD model of that turbine could not be found. However, for an actuator disk model, a CAD model is not used. The wind turbine was designed so that the results could be validated using the NREL results and the results of a 2010 CFD study conducted by the University of Massachusetts-Amherst by a researcher name Dnyanesh A. Digraskar [10].

In the UMass-Amherst study, a 5m long blade was rotating at 72 RPM with free stream velocities that ranged from 7.0 m/s to 25.0 m/s. The blade used in the study was the NREL blade, which utilized the S809 airfoil. For this research, a wind turbine with three

blades was used, but the blades were the same ones that were used in the UMass-Amherst study. This was done in order to determine how the result would vary given that the entire turbine was modeled as opposed to just a single blade. The Star-CCM+ virtual disk model was used to conduct this study.

Star-CCM+ Virtual Disk Model

The virtual disk model on Star-CCM+ is a useful tool for modeling a wind turbine because all of the information about the turbine can be entered in, such as the lift and drag coefficients, the airfoil chord length, the angle of twist, the sweep angle distribution and the number and length of the blades.

There are three different methods that can be implemented within the virtual disk model, body force propeller method, 1D momentum method and blade element method. The first is not applicable to wind turbines because it is designed to model systems similar to marine propellers, in which the flow around the ship, the propeller and the flow induced by the propeller are all modeled [15]. This is a very different situation than a wind turbine, where only the flow around the turbine and the rotation of the turbine need to be analyzed. Blade element method and 1D momentum theory are both applicable to modeling horizontal axis wind turbines, as these theories are both commonly used to analyze wind turbines outside of computational fluid models.

The 1D momentum theory was designed specifically for the purpose of modeling a HAWT. The method accounts for the axial and tangential effects of the wind turbine in the flow, thus mimicking the wind turbine. The benefit of this model is that it is specifically designed to model wind turbines and therefore the wake produced as a result of this method

are reliable and accurate. The downside of this model is that, one of the inputs required to run the simulation is a power curve for the turbine [15]. Therefore, this method cannot be used to determine the power generated by a single turbine. Instead, this method is used to study the wake of a wind turbine and to model wind farms. In order to maximize the power generated by a wind farm, the turbines should not interfere with one another, meaning a turbine should not lie in the wake of another turbine. Using this tool, a number of wind turbines can be modeled and their layout can be adjusted until each wind turbine is operating most efficiently and the energy production of the entire wind farm is maximized.

The goal of this research was to determine the power generated by a wind turbine through computational fluid models, therefore the best method for this purpose is the blade element method. The initial purpose for this method was to be able to accurately capture the wake produced by helicopter rotors and the interaction between the rotor wakes [15]. However, wind turbine rotors behave similarly to helicopter rotors and the wakes created by each have similar characteristics. Moreover, blade element method is commonly used in the design of wind turbine blades and the analysis of the power generated by wind turbines. The wind turbine is modeled as a distribution of momentum sources and the lift and drag coefficients, as well as other geometric characteristics of the blade, are used to model the behavior of the blade and the fluid around the blade.

Geometry

The turbine that was selected for this simulation had three blades with an outer radius of 5.0 m, an inner radius of 0.25 m (the inner radius is the radius of the rotor hub) and the thickness of the virtual disk was set at 0.25 m. Although the physical turbine is not

meshed in an ADM simulation, the simulation is very accurate because it requires input data about the airfoil used for the blade. In this case the S809 airfoil was used, the shape of which is shown below in figure 16. All the information regarding the S809 airfoil was obtained from the NREL Information Portal [18].

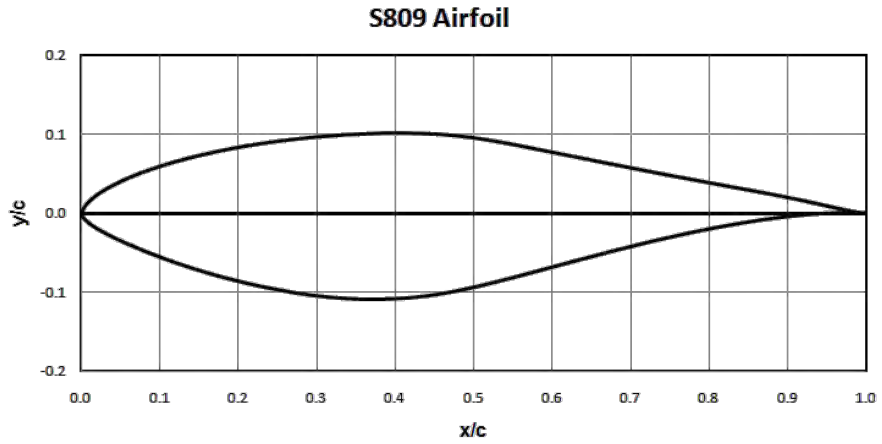

Figure 16: S809 airfoil, used for the shape of the blades of the wind turbine used in this research [18].

A table of the coefficients of lift and drag and angles of attack at a Reynolds number of 500,000 and Mach 0, which was also obtained from the NREL website, was applied to this simulation. The table is attached in appendix 1.

The chord length of the S809 airfoil used in the NREL study and the UMass-Amherst study varied along the blade, but to simplify this model, the chord length was held constant. The average chord length for the blade in the other two studies was calculated to be 0.505 m and that value was used for the constant chord length in this study. A constant twist of 4 degrees was also determined from the other two studies.

Appendix 1 contains the table that was used to determine these values and a table containing the information about the geometry of the turbine [10].

Physics and Mesh Continua

For these models, the physics conditions were slightly different than in the previous two models. The flow was steady and turbulent, the RANS equations were applied and the model was three dimensional, but the ideal gas law was used to model the air rather than assuming the air was constant density. This was done because there was an error with the simulation when the flow was defined as incompressible. Although it initially seemed like an issue that the flow was not constant density, it was later confirmed that the density was barely changing, which will be proved in later sections. Finally, the turbulence model used for this study was standard Spalart-Allmaras, which was used for the UMass-Amherst study.

An automated mesh was generated for this model, which used a surface remesher and a polyhedral mesher with a base size of 2.0 m. A volumetric control for the virtual disk was created that had a base size of 1.0 m.

Boundary, Initial Conditions and Rotation

The same three boundary conditions of velocity inlet, pressure outlet and slip wall were set for the background region in this study. The inlet velocity was first set to 7.0 m/s and then the study was conducted again with an inlet velocity of 15.0 m/s. The initial velocity was set to match the inlet velocity and it was constrained to be in the z-direction. As in the other simulations, the rotation rate for the wind turbine was set to 72 RPM.

Results

Different velocity and pressure scenes were created in order to get a clearer picture of the flow. Figure 17 shows the velocity at the front and back of the virtual disk with a free stream velocity of 7.0 m/s and 15.0 m/s.

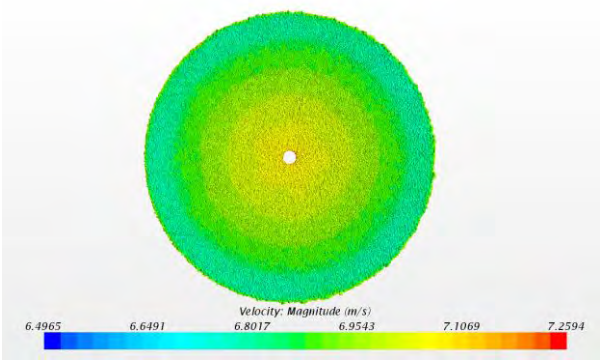

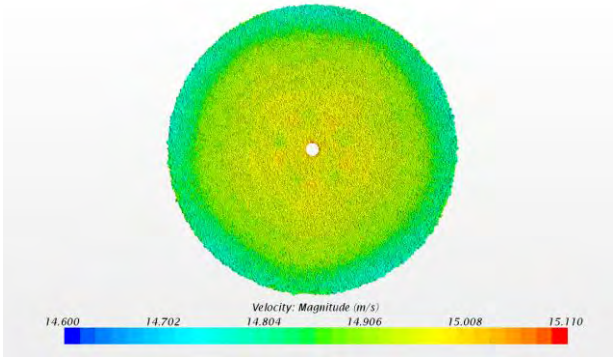

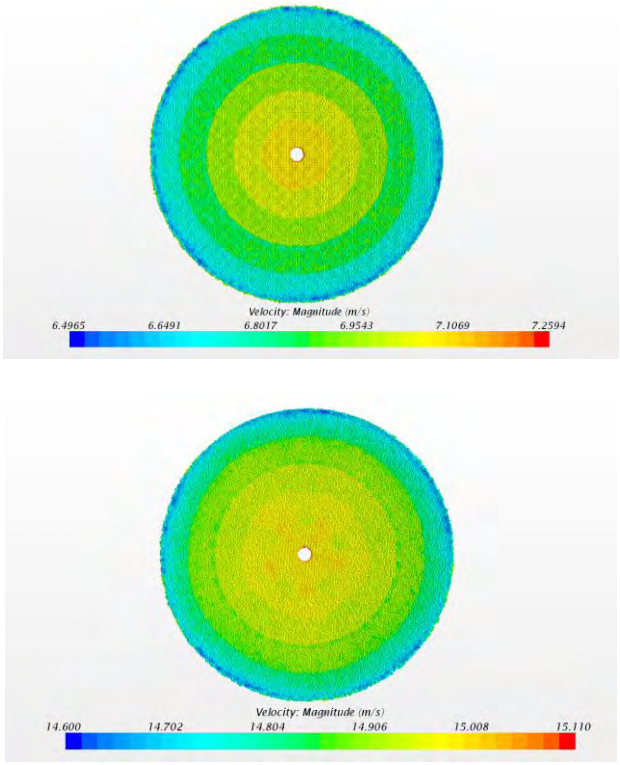

Figure 17: [Left] The top image shows the velocity of the flow around the front face of the turbine when the free stream is 7.0 m/s. The bottom velocity contour is also for a free stream velocity of 7.0 m/s, but on the back face of the turbine. [Right] The top and bottom correspond to the front and back of the turbine, respectively, with a free stream velocity of 15.0 m/s.

As expected, the velocity of the flow decreases at the front of the turbine in both cases. Something interesting to note is that the region of slower velocity is larger in the 15.0 m/s case, but this difference is very slight. One possible reason for this is that, since the fluid is moving faster, when it hits the turbine it does not have enough time to change direction, quickly and flow around the turbine, therefore a larger region of it slows down than in the slower moving study.

The pressure contour for the study with a free stream velocity of 7.0 m/s is shown in figure 18. The vertical line where the color changes from orange to green and blue in

the picture is where the turbine is located. The pressure contour for the 15.0 m/s study was very similar, it can be seen in appendix 3.

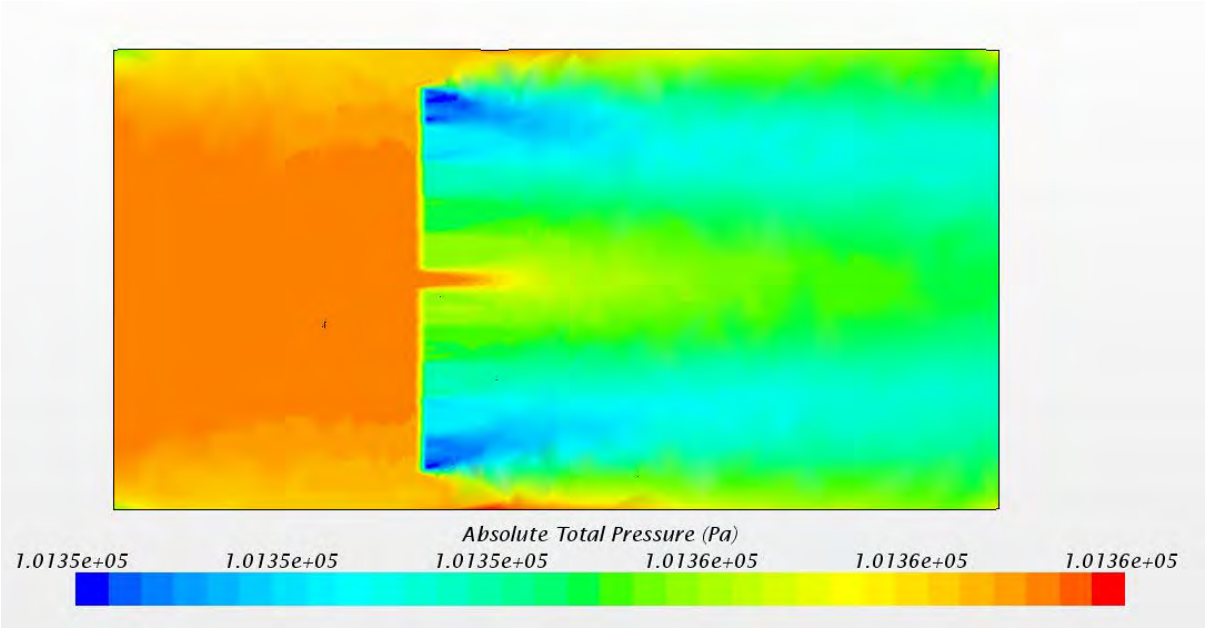

Figure 18: Pressure contour for the actuator disk model with a free stream velocity of 7.0m/s.

The pressure in front of the turbine is shown to be higher than behind the turbine, and it greatly decreases above and below the turbine. This decrease in pressure above and below the turbine occurs because the flow slows down in that region.

As stated earlier, this study was unable to be conducted using an incompressible model, even though the density should not be changing much around such a small, slow moving turbine. A density contour was created, which showed that, although the density was not completely constant, there was very little change in the density throughout the flow. Further analysis of the results shows that the minimum density was 1.17666 kg/m^2 and the maximum density was 1.17673 kg/m^3. The density contour plot is shown in appendix 3

Figure 19 shows the velocity in the wake of the turbine for the simulation with a free stream velocity of 7.0m/s.

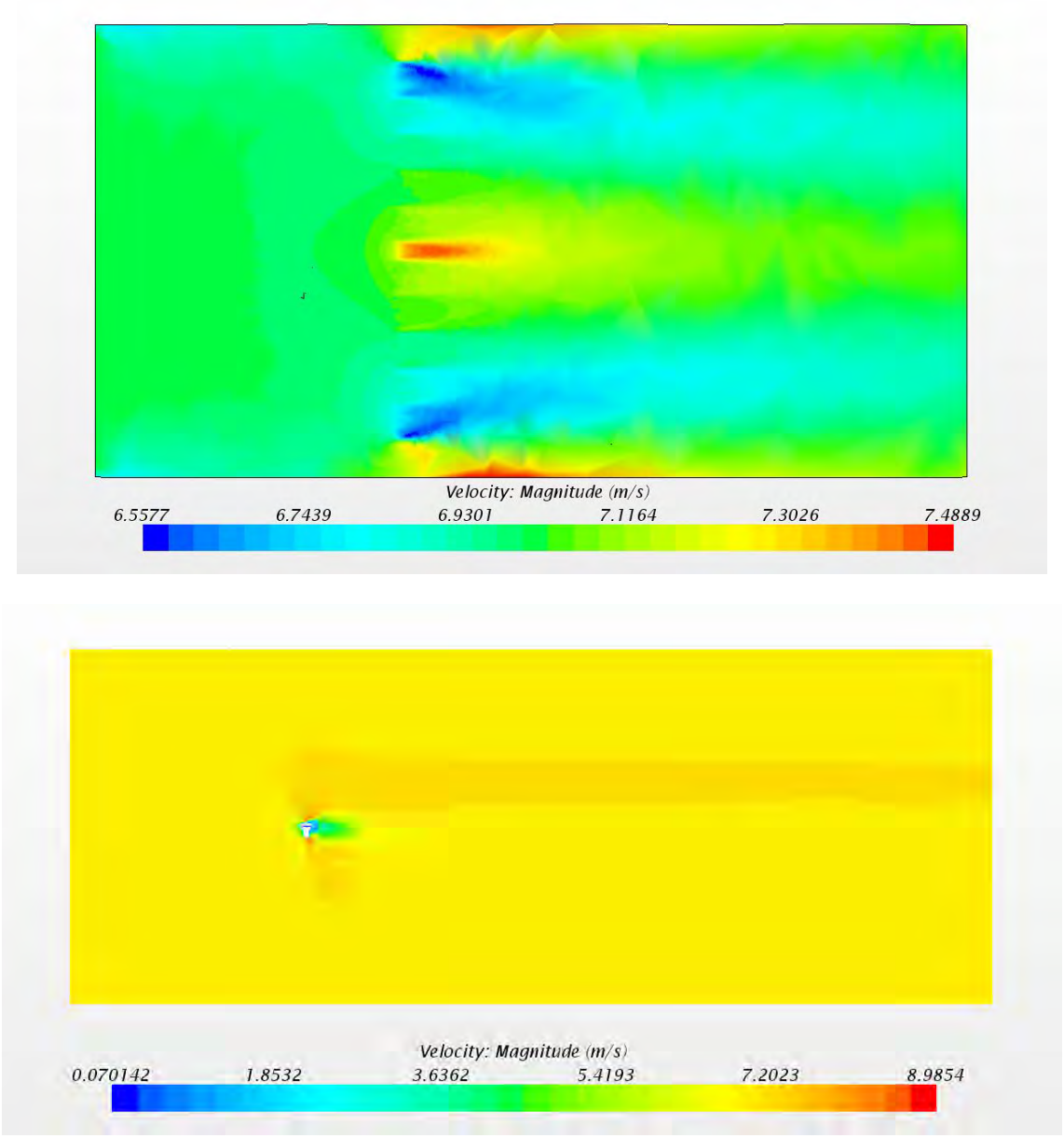

Figure 19: Comparison between ADM velocity wake and RBM velocity wake at same free stream velocity. [Top] Velocity contour for the actuator disk model with a free stream velocity of 7.0m/s. [Bottom] Velocity contour from the rigid body motion simulation with a free stream velocity of 7.0m/s.

From the top image in the figure, it is clear that regions of low velocity and regions of low pressure overlap, which is the same result that was determined from the previous models.

Immediately behind the turbine, the velocities and pressure vary greatly in the vertical direction, but farther away from the turbine, the flow becomes more uniform. This varying flow is the turbine's wake and when the wake ends, the flow becomes uniform once again, which is shown in the figure.

In the center of the virtual disk, there is a small hole through which the fluid can pass, it is shown in figure 18 by the strip of orange that extends farther past the turbine than the rest and in figure 19 by the small patch of red in the middle of the contour. While this is accurate for the virtual disk model, it would not occur in a real wind turbine because that is where the hub is located. The bottom image in figure 19 is the velocity contour from the rigid body motion simulation with a free stream velocity of 7.0m/s. In the pressure and velocity contours from the rigid body motion study, this region directly behind the hub is a region of low pressure and velocity, opposite to the ADM result.

Figure 20 shows a velocity wake determined through an LES model by the Wind Engineering and Renewable Energy Lab (WIRE) in Lausanne, Switzerland [19]. The wake is a triangular region of low velocity that tapers behind the turbine as the flow speeds back up.

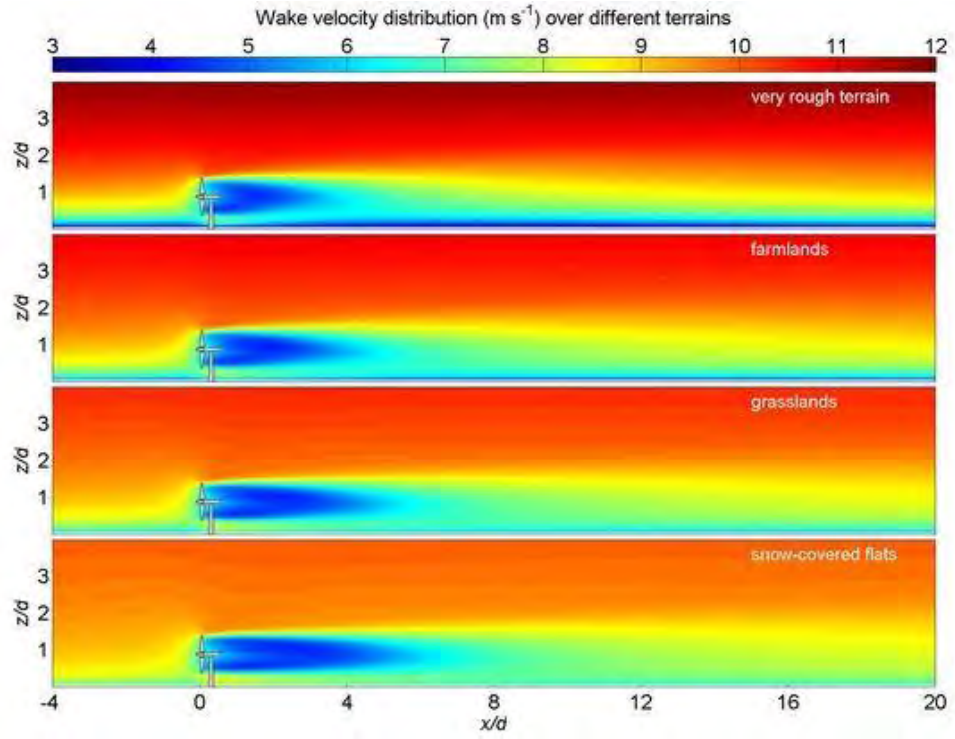

Figure 20: Wake velocity of wind turbines, determined through and LES model by the Wind Engineering and Renewable Energy Lab (WIRE) in Lausanne, Switzerland [19].

This triangular shaped wake can also be seen in the results determined through the ADM simulation, though it is less defined than the wake in the WIRE study.

The next step was to calculate the power generated by the turbine based on the results found in this study. This was again done by determining the torque caused by the fluid acting on the turbine. Table 2 lists the values of for torque, angular velocity and power generated in each condition.

Table 2: Power generated by a HAWT under different free stream velocities, determined using an actuator disk model

Condition (Free stream velocity)	Torque	Angular Velocity	Power Generated
7.0 m/s	268.57 Nm	72 RPM (7.54 rad/s)	20.25 kW
15.0 m/s	965.28 Nm	72 RPM (7.54 rad/s)	72.78 kW

Validation

The UMass Amherst study, which tested only the blades rather than the entire turbine, compared results obtained through CFD studies to NREL results. Their results are shown in figure 21.

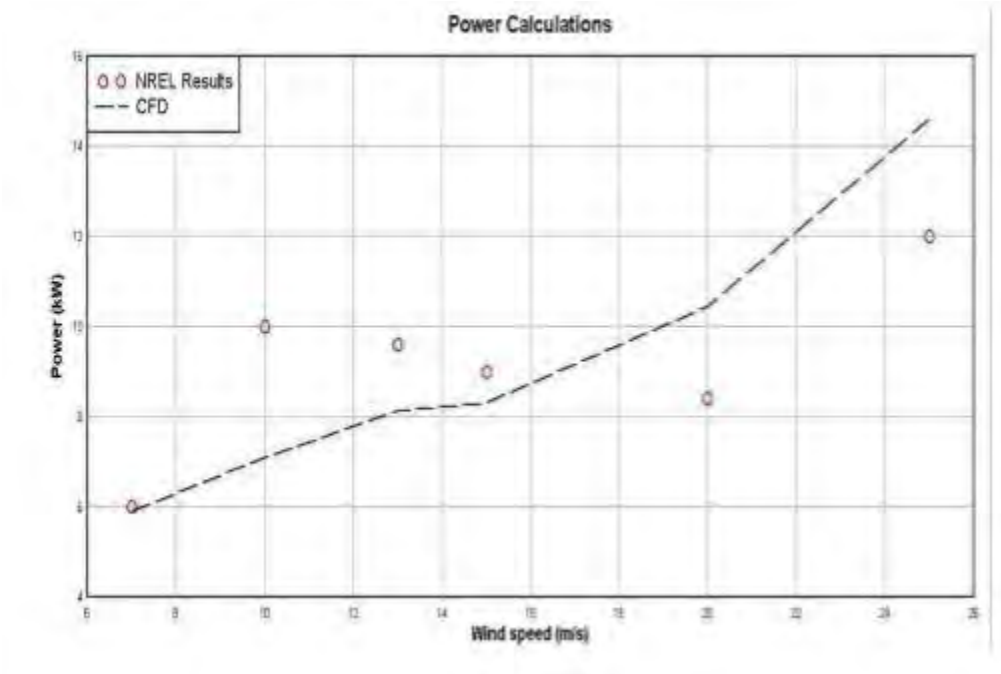

Figure 21: Power generated by HAWT, determined through CFD studies conducted at the University of Massachusetts-Amherst and experimentally by the National Renewable Energy Laboratory [10].

The UMass-Amherst computational study determined that the power produced by the HAWT at a wind speed of 7.0 m/s was about 6 kW and about 8.5 kW at 15.0 m/s. The NREL results were the same at 7.0 m/s, but at 15.0 m/s the experimental value for power generated was 9.0 kW. The values for power generated determined by this research were significantly higher than published values, which could be due to the turbine being modeled as an actuator disk. Simplifying the geometry to a disk omits the need for a complex mesh but, to an extent it also limits the accuracy.

Turbulence Model Comparison Study:

For all of the previously mentioned studies, the Spalart-Allmaras RANS turbulence model was applied in order to control some of the variation between the models. This model was initially chosen because it was used in the UMass-Amherst study and it was determined that, in order to accurately validate the study, it was best to use the same turbulence model. Although applying this model to a full wind turbine is not incorrect, the Spalart-Allmaras model is most frequently used for flow over airfoils and blades. Moreover, this model has difficulty dealing with complex recirculation in the flow, indicating it might not be the best choice for a wind turbine model. In order to determine the differences between the three most common turbulence models, namely Spalart-Allmaras, k-epsilon and k-omega, three actuator disk model studies were carried out in which everything but the turbulence model was kept the same. The free stream velocity for these studies was set at 7.0 m/s, and then the same comparison study was carried out at 15.0 m/s. Table 3 shows the results of the power calculations for these six studies.

Table 3: Calculations for power generated by a wind turbine using different turbulence models

Turbulence Model	Free-Stream Velocity (m/s)	Torque (Nm)	Power (kW)
Spalart-Allmaras	7.0	268.57	20.25
	15.0	965.29	72.78
k-Epsilon	7.0	271.14	20.44
	15.0	971.79	73.27
k-Omega	7.0	271.14	20.44
	15.0	971.79	73.27

The values determined using the k-omega and k-epsilon turbulence models are the same, but they differ from the values determined by the spalart-allmaras model. One possible reason for this is that the k-omega and k-epsilon models are inherently more similar to each other than to the spalart-allmaras model because they are both two equation models, as opposed to a one-equation model. They are not significantly different though, so it does not appear that they are any more or less accurate than the original model.

The contour plots for the three different turbulence models produced the same results. It was expected that the vorticity contour plot for the spalart-allmaras model would be the only plot that would show significant differences because that model isn't as accurate when measuring vorticity, however the contour plots were nearly identical. Figure 22 shows the vorticity contour plot for each of the turbulence models at 15.0 m/s.

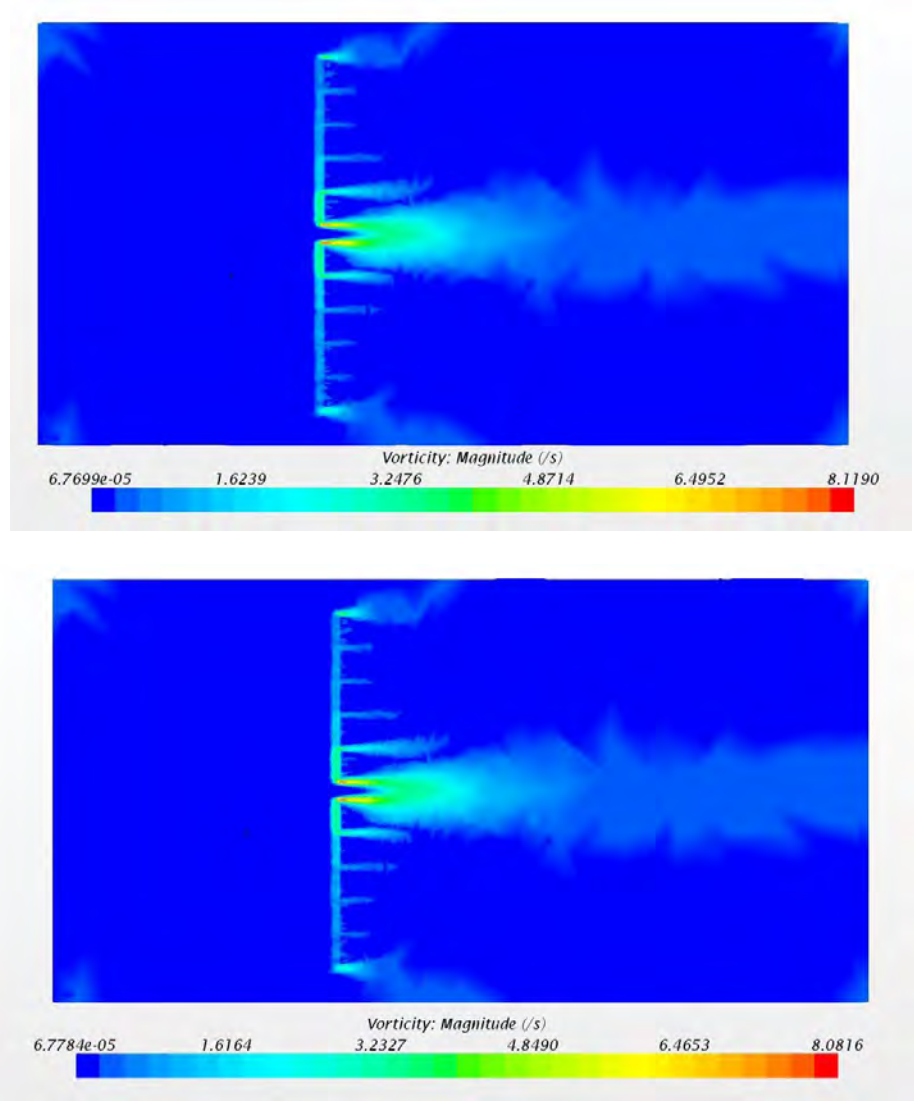

Figure 22: Vorticity contour plot for the k-epsilon turbulence model [top] and the spalart-allmaras model [bottom]. Both are for a free stream velocity of 15.0 m/s.

The vorticity contour for the k-omega contour plot is not pictured because it was identical to the other two. A vorticity plot is useful because vorticity is a measure of the rotation in the flow, thus in this plot the areas of green and yellow depict where there is the most rotation within the fluid. The virtual disk used to model the turbine is porous, therefore

the little tube-like shapes of high vorticity that appear to pass through the turbine are actually the fluid passing through the pores in the disk.

Conclusions and Recommendations:

Three different types of computational fluid dynamic studies were conducted to model horizontal axis wind turbines; rigid body motion, dynamic fluid body interaction and actuator disk model. Of these three simulations it was determined that actuator disk model was the best because the fluid wake in these studies most closely resembled published results. Moreover, the DFBI model was not able to accurately capture and mimic the rotation of the fluid. While the rigid body motion study did not accurately model the wake, the power output calculated was within the realm of possibility because it was on the same scale of magnitude as the published values that were used for validation.

In order to carry out a proper validation study for the rigid body motion simulation, a CAD model should be used that already has been tested experimentally or by other researchers. This would be beneficial because, although similar size turbines should be generating similar magnitudes of power, there can still be vast differences in the exact value due to the design of the blades. It is plausible that one turbine could generate 100 W, while a different turbine with the same radius might generate only 20 W. Therefore, in order to determine the accuracy of this model, a turbine with known or estimated power generation values should be modeled. Ideally this should be done with the NREL turbine because there is a large amount of published research regarding the power generation of this turbine in various conditions. A CAD model of the NREL

turbine could not be obtained and there was not enough time within the duration of this research to create a CAD model to match the NREL turbine, therefore a generic horizontal axis wind turbine CAD model was used.

Although the calculated values for power generated by the wind turbines did not exactly match published values, they were within the same magnitude. In order to improve these models, some inputs for the study can be further defined, such as turbulent viscosity ratio and other flow characteristics. Defining as many inputs as possible will certainly improve the accuracy of the CFD studies.

It can also be concluded that, although the dynamic fluid body interaction model makes the most sense theoretically because the rotation of the turbine is driven by the flow, it is much more complicated to execute. Though many iterations were conducted, none of the DFBI studies in this research were successful. One reason for this is that the simulation may have required more computational power than was available. For example, the DFBI simulations were run overnight for nearly 5000 iterations and yet the solutions did not converge. Had more computing power been available, the simulations could have been run for longer amounts of time to improve the results. This was not able to be tested, so it is unclear whether more solution time would have had an impact on the results. Therefore, models that require the rotation rate to be set are recommended over DFBI models because they are more accurate and simpler than DFBI models.

Future Work:

Throughout this study, only horizontal axis wind turbines were modeled. This was done purposely because they are far more common and, at the large scale, they're

typically more efficient than vertical axis wind turbines. However, at the small scale, horizontal axis wind turbines do not always outperform the vertical axis models. In fact, some small vertical axis turbines are more efficient. It would be beneficial to model some vertical axis wind turbines in order to examine the difference between the two. The virtual disk model is specifically set up for horizontal axis turbines, but it might be possible to manipulate the inputs enough to behave like a vertical axis turbine. If this proved impossible, the rigid body motion model would be a viable option.

The 1D momentum method in the virtual disk model would also be worth exploring. It was not used during this research because a power curve for the turbine being modeled is one of the inputs and the goal of this research was the determine the power generated by a wind turbine. However this tool could be used to validate studies conducted using the methods in this research. For example, a turbine could be modeled using blade element method and 1D momentum method. The 1D momentum method would generate an accurate wake for the turbine, which could then be compared to the wake generated using the blade element method. The results should be the same because both of these theories are frequently used to analyze wind turbines.

In addition, the 1D momentum method could be used to model a wind farm. This would be a more complicated simulation and it would require a large amount of computing power, but the benefit is that the power generated by a number of turbines could be determined as compared to the power generated by one.

The purpose of this research was to model small-scale wind turbines, however the turbine that was modeled using actuator disk method was about 10 meters in diameter. While this is still not a huge turbine, it is larger than most that would be found in a

residential setting. Therefore, once the actuator disk model is validated and determined to be accurate, this turbine could be scaled down to half, or a quarter of the size. This smaller size would be beneficial to analyze because it would resemble the size of a turbine found in a residential setting, and could be used to determine the benefit of a small-scale wind turbine.

Another step of this research could be to look at the effects of the tips of the blades in the flow and the vortices they create. This was not done in this research because the focus was on the overall behavior and characteristics of the wake. However, the analysis of these vortices could be carried out by implementing an actuator line model rather than an actuator disk model. Like ADM, ALM simplifies the geometry of the turbine while maintaining the accuracy, but it models the turbine as rotating lines rather than a rotating disk. Star-CCM+ does not have a built in tool for an actuator line model, so it would require more work to set up, but it would be a beneficial next step for this research.

References

[1] "Wind Flow Under Complex Terrain (CFD)," *MegaJoule,* 2016. [Online]. Available: http://www.megajoule.pt/nm_quemsomos.php?id=180. [Accessed: 18-Nov-2016].

[2] "Predicting Wind Power with Greater Accuracy – S&TR," Apr-2012. [Online]. Available: https://str.llnl.gov/content/pages/april-2014/pdf/04.14.1.pdf. [Accessed: 18-Nov-2016].

[3] A. A. Makky, "Navier-Stokes Equations," *Computational Fluid Dynamics is the Future,* 2012. [Online]. Available: http://cfd2012.com/navier-stokes-equations.html. [Accessed 18-Nov-2016].

[4] Lynch, E., 2011, "Advanced CFD Methods for Wind Turbine Analysis," Ph.D. thesis, School of Aerospace Engineering, Georgia Institute of Technology.

[5] Salim, S. M., Ong, K. C., Cheah, S. C., 2011, "Comparison of RANS, URANS and LES in the Prediction of Airflow and Pollutant Dispersion," Proceedings of the World Congress on Engineering and Computer Science, vol. 2, San Francisco.

[6] S. Som, D. Longman, Z. Luo, M. Plomer, T. Lu, P. Senecal, and E. Pomraning, "Simulating Flame Lift-Off Characteristics of Diesel and Biodiesel Fuels Using Detailed

Chemical-Kinetic Mechanisms and Large Eddy Simulation Turbulence Model," *Journal of Energy Resources Technology,* vol. 134, no. 3, Aug. 2012.

[7] Martinez Tossas, L.A., Leonardi, S., 2013, "Wind Turbine Modeling for Computational Fluid Dynamics," NREL/SR-5000-55054, National Renewable Energy Laboratory, Golden, CO.

[8] Sumner, J., Warrets, C.S., Masson, C., 2010, "CFD in Wind Energy: The Virtual, Multiscale Wind Tunnel," Energies, vol. 3, pp. 990-1013.

[9] Information from Star-CCM+ tutorials

[10] D. A. Digraskar, "Simulations of flow over wind turbines," thesis 2010. University of Massachusetts – Amherst.

[11] C. E. Carcangiu, "CFD-RANS Study of Horizontal Axis Wind Turbines," thesis, 2008. Universita Degli Studi di Cagliari.

[12] R. S. Jackson, "Application of the Reynolds Stress Model Using Direct Modeling and Actuator Disk Approaches for a Small-Scale Wind Turbine," thesis, 2016. University of Wisconsin – Milwaukee.

[13] V. Sharma, GrabCAD – CAD library. [Online]. Available: https://grabcad.com/library/windmill-13. [Accessed: 09-DEC-2016].

[14] H. Cao, "Aerodynamic Analysis of Small Horizontal Axis Wind Turbine Blades by Using 2D and 3D CFD Modelling," thesis, 2011. University of Central Lancashire.

[15] Star-CCM+ User Guide.

[16] M. M. Hand, D. A. Simms, L. J. Fingersh, D. W. Jager, J. R. Cotrell, S. Schreck, and S. M. Larwood, "Unsteady Aerodynamics Experiment Phase VI: Wind Tunnel Test Configurations and Available Data Campaigns," *National Renewable Energy Laboratory*, Jan. 2001.

[17] M. Refan and H. Hangan, "Aerodynamic Performance of a Small Horizontal Axis Wind Turbine," *Journal of Solar Energy Engineering,* vol. 134, no. 2, May 2012.

[18] J. M. L. Buhl, "S809 Airfoil Shape," *NWTC Information Portal*. [Online]. Available: https://wind.nrel.gov/airfoils/shapes/S809_Shape.html. [Accessed: 2-Feb-2017]

[19] Y. T. Wu and F. Porte-Agel, "Atmospheric Turbulence Effects on Wind-Turbine Wakes: An LES Study," *Energies*, vol. 5, no. 12, pp. 5340-5362, 2012.

[20] NREL's S809 Airfoil (s809-nr). [Online]. Available: http://airfoiltools.com/airfoil/details?airfoil=s809-nr. [Accessed: 20-Feb-2017].

Appendix 1: Actuator Disk Model Turbine geometry

Table 1: S809 Airfoil Data [20]

Polar key	xf-s809-nr-500000					
Airfoil	s809-nr					
Reynolds number	500000					
Ncrit	9					
Mach	0					
Max Cl/Cd	81.2007					
Max Cl/Cd alpha	7					
Alpha (angle of attack)	Cl	Cd	Cdp	Cm	Top_Xtr	Bot_Xtr
-18	-0.3992	0.16006	0.15751	-0.0156	0.772	0.0155
-17.75	-0.4079	0.15215	0.14959	-0.0203	0.7665	0.0161
-11.5	-0.6189	0.04377	0.03655	-0.0617	0.6633	0.0097
-11.25	-0.586	0.04451	0.03728	-0.0603	0.6604	0.0101
-11	-0.5621	0.04466	0.03741	-0.0591	0.658	0.0102
-10.75	-0.5447	0.04405	0.03677	-0.0587	0.6559	0.0105
-10.5	-0.5268	0.04369	0.03639	-0.0577	0.6537	0.0106
-10.25	-0.5115	0.04291	0.0356	-0.0573	0.6518	0.0112
-10	-0.4961	0.04213	0.03478	-0.0569	0.65	0.0117
-9.75	-0.4845	0.0413	0.03392	-0.0557	0.6483	0.0118
-9.5	-0.4724	0.04032	0.03288	-0.0551	0.6467	0.0122
-9.25	-0.4626	0.03919	0.03171	-0.0543	0.6452	0.0121
-9	-0.4523	0.03806	0.03053	-0.0537	0.6436	0.0124
-8.75	-0.4464	0.03661	0.02905	-0.0528	0.6425	0.0124
-8.5	-0.4437	0.03492	0.02734	-0.0517	0.6413	0.0129
-8.25	-0.4412	0.03328	0.02568	-0.0506	0.64	0.0134
-8	-0.4363	0.03183	0.02422	-0.0495	0.6387	0.0149
-7.75	-0.4298	0.03055	0.0229	-0.0485	0.6376	0.015

-7.5	-0.4241	0.02926	0.02156	-0.0474	0.6365	0.016
-7.25	-0.4247	0.0276	0.01988	-0.0458	0.6354	0.0184
-7	-0.4257	0.02592	0.01819	-0.0441	0.6344	0.024
-6.75	-0.4352	0.02378	0.01612	-0.0417	0.6334	0.0433
-6.5	-0.4597	0.02075	0.01327	-0.0383	0.6325	0.0911
-6.25	-0.4872	0.01788	0.01051	-0.0341	0.6316	0.1316
-6	-0.5147	0.01444	0.00733	-0.0314	0.6307	0.225
-5.75	-0.5255	0.01121	0.00508	-0.0294	0.6298	0.4604
-5.5	-0.4954	0.01172	0.00554	-0.03	0.6288	0.487
-5	-0.4319	0.01373	0.00765	-0.0307	0.6271	0.5106
-4.75	-0.4013	0.01452	0.00838	-0.0311	0.6265	0.5184
-4.5	-0.3701	0.01496	0.0089	-0.0315	0.6258	0.5212
-4.25	-0.3414	0.01485	0.00874	-0.0321	0.6251	0.5221
-4	-0.3126	0.01475	0.00859	-0.0327	0.6244	0.523
-3.75	-0.2838	0.01465	0.00844	-0.0333	0.6237	0.5239
-3.5	-0.255	0.01455	0.0083	-0.034	0.6231	0.525
-3.25	-0.2262	0.01445	0.00815	-0.0346	0.6222	0.5261
-3	-0.1974	0.01435	0.008	-0.0353	0.6213	0.5272
-2.75	-0.1685	0.01426	0.00787	-0.0359	0.6205	0.5285
-2.5	-0.1395	0.01419	0.00775	-0.0366	0.6198	0.5299
-2.25	-0.1105	0.01414	0.00764	-0.0373	0.6192	0.5311
-2	-0.0814	0.01409	0.00754	-0.038	0.6185	0.5321
-1.75	-0.0524	0.01399	0.00739	-0.0387	0.6179	0.5331
-1.5	-0.0235	0.01383	0.00724	-0.0394	0.6173	0.5341
-1.25	0.0056	0.01377	0.00719	-0.04	0.6168	0.535
-1	0.0348	0.01376	0.00718	-0.0407	0.6162	0.5359
-0.75	0.0641	0.01376	0.00719	-0.0413	0.6157	0.5368
-0.5	0.0934	0.01378	0.00721	-0.042	0.6151	0.5377
-0.25	0.1226	0.01381	0.00724	-0.0426	0.6145	0.5387

0	0.1519	0.01386	0.00729	-0.0433	0.6137	0.5398
0.25	0.1812	0.01394	0.00738	-0.0439	0.613	0.541
0.5	0.2103	0.01404	0.00749	-0.0446	0.6125	0.5423
0.75	0.2394	0.01415	0.00761	-0.0453	0.6119	0.5435
1	0.2685	0.01415	0.00764	-0.0459	0.6113	0.5446
1.25	0.2975	0.01414	0.00765	-0.0466	0.6103	0.5457
1.5	0.3265	0.01415	0.00769	-0.0472	0.6092	0.5467
1.75	0.3555	0.0142	0.00776	-0.0478	0.6081	0.5476
2	0.3844	0.01419	0.00778	-0.0485	0.6071	0.5485
2.25	0.4131	0.01415	0.00781	-0.049	0.6059	0.5497
2.5	0.4418	0.01418	0.00791	-0.0496	0.6048	0.5508
2.75	0.4706	0.01423	0.00803	-0.0501	0.6035	0.5519
3	0.4996	0.01426	0.00812	-0.0506	0.6019	0.553
3.25	0.5289	0.01426	0.00815	-0.0511	0.5999	0.5541
3.5	0.5584	0.01429	0.00819	-0.0517	0.5978	0.5552
3.75	0.5871	0.01439	0.00833	-0.0522	0.5951	0.5563
4	0.6152	0.01425	0.00827	-0.0525	0.5914	0.5575
4.25	0.6442	0.01407	0.00813	-0.0529	0.587	0.5586
4.5	0.6745	0.01386	0.0079	-0.0534	0.5827	0.5598
4.75	0.7033	0.01378	0.00784	-0.0538	0.5781	0.5611
5	0.731	0.01353	0.00766	-0.0539	0.5719	0.5623
5.25	0.761	0.01332	0.00744	-0.0544	0.5671	0.5633
5.5	0.7893	0.01315	0.00732	-0.0547	0.5626	0.5645
5.75	0.816	0.01285	0.00716	-0.0546	0.556	0.5657
6	0.8446	0.01254	0.00685	-0.0548	0.5486	0.5668
6.25	0.8703	0.01229	0.00676	-0.0545	0.5398	0.5679
6.5	0.897	0.01207	0.00662	-0.0544	0.5305	0.569
6.75	0.9232	0.01187	0.00654	-0.0541	0.5162	0.5702
7	0.9468	0.01166	0.00632	-0.0534	0.4731	0.5715

7.25	0.9485	0.0126	0.0067	-0.0492	0.3779	0.5727
7.5	0.9493	0.01382	0.00754	-0.0451	0.3042	0.5739
7.75	0.9494	0.01493	0.00835	-0.0411	0.2451	0.5751
8	0.9473	0.01583	0.00904	-0.0366	0.2033	0.5763
8.25	0.9442	0.01675	0.0098	-0.032	0.169	0.5772
8.5	0.9435	0.01782	0.01072	-0.0283	0.14	0.5781
8.75	0.9435	0.01897	0.01176	-0.0251	0.1163	0.5788
9	0.9437	0.02018	0.0129	-0.0223	0.0961	0.5801
9.25	0.9448	0.02155	0.01422	-0.0201	0.0805	0.5812
9.5	0.9477	0.02302	0.01566	-0.0184	0.0669	0.5823
9.75	0.9512	0.02458	0.01721	-0.0169	0.0563	0.5835
10	0.9567	0.02611	0.01873	-0.0158	0.0481	0.5846
10.25	0.9638	0.02757	0.02022	-0.0148	0.0423	0.5859
10.5	0.9668	0.02935	0.022	-0.0136	0.0374	0.5871
10.75	0.977	0.03062	0.02334	-0.0129	0.0343	0.5884
11	0.9827	0.03225	0.02496	-0.012	0.031	0.5899
11.25	0.9887	0.03388	0.02664	-0.0112	0.0286	0.5913
11.5	0.9974	0.03533	0.02815	-0.0105	0.0269	0.5926
11.75	1.0044	0.03694	0.02977	-0.0099	0.025	0.5939
12	1.0031	0.03921	0.03208	-0.0088	0.0234	0.5951
12.25	1.0132	0.04059	0.03358	-0.0084	0.0226	0.5966
12.5	1.022	0.04212	0.0352	-0.008	0.0215	0.598
12.75	1.0304	0.04374	0.03688	-0.0076	0.0205	0.5995
13	1.0371	0.04554	0.03873	-0.0072	0.0196	0.6009
13.25	1.0364	0.04803	0.04126	-0.0066	0.0185	0.6024
13.5	1.0452	0.04976	0.04308	-0.0064	0.018	0.6039
13.75	1.0549	0.05145	0.04485	-0.0063	0.0173	0.6057
14	1.0626	0.05334	0.04683	-0.0062	0.0167	0.6073
14.25	1.0713	0.05522	0.04876	-0.0062	0.016	0.6089

14.5	1.0799	0.05712	0.0507	-0.0065	0.0151	0.6107
14.75	1.0838	0.05949	0.05315	-0.0065	0.0147	0.6124
15	1.0866	0.06199	0.05576	-0.0063	0.0141	0.6142
15.25	1.0952	0.06406	0.05795	-0.0067	0.0136	0.6163
15.5	1.1021	0.06635	0.06036	-0.0071	0.0131	0.6185
15.75	1.1082	0.06877	0.06286	-0.0076	0.0126	0.6209
16	1.1149	0.0712	0.06535	-0.0084	0.012	0.6232
16.25	1.1188	0.07394	0.06815	-0.0091	0.0116	0.6254
16.5	1.1171	0.07737	0.07165	-0.0098	0.0109	0.6275
16.75	1.1216	0.08027	0.0747	-0.0107	0.0106	0.63
17	1.1255	0.08335	0.07794	-0.0119	0.0102	0.6326
17.25	1.1276	0.08669	0.08141	-0.0131	0.0098	0.6352
17.5	1.1296	0.09009	0.08491	-0.0145	0.0094	0.6381
17.75	1.1308	0.09372	0.08862	-0.0161	0.0091	0.6408
18	1.1307	0.09757	0.09259	-0.0178	0.0088	0.6437
18.25	1.1292	0.10166	0.09679	-0.0196	0.0086	0.6466
18.5	1.1243	0.1063	0.10154	-0.0216	0.0084	0.6497
18.75	1.1179	0.11131	0.10668	-0.0239	0.0081	0.6526

Table 2: Blade Chord and Twist Configuration from UMass-Amherst and NREL Studies [10]

Radial Dist. (m)	Chord (m)	Twist (degrees)	Twist (rads)
0	hub diameter	0	0
0.724	hub diameter	0	0
0.838	to be computed	30	0.523598776
0.968	to be computed	27.59	0.481536341
1.258	0.737	20.05	0.349938515

1.522	0.71	14.04	0.245044227
1.798	0.682	9.67	0.168773339
2.075	0.654	6.75	0.117809725
2.352	0.626	4.84	0.084473936
2.628	0.598	3.48	0.060737458
2.905	0.57	2.4	0.041887902
3.181	0.542	1.51	0.026354472
3.458	0.514	0.76	0.013264502
3.735	0.486	0.09	0.001570796
2.772	0.483	0	0
4.011	0.459	-0.55	-0.009599311
4.288	0.431	-1.11	-0.019373155
4.565	0.403	-1.55	-0.027052603
4.841	0.375	-1.84	-0.032114058
5.03	0.356	-2	-0.034906585
5.118	0.347	-2.08	-0.036302848
5.395	0.319	-2.36	-0.04118977
5.533	0.305	-2.5	-0.043633231

Table 3: Turbine geometry used in the actuator disk model

Number of blades	3
Outer radius	5.0 m
Inner radius	0.25 m
Airfoil	S809
Chord length	0.505 m
Angle of twist	4 degrees

Appendix 2: Additional images from the Dynamic Fluid Body Interaction Study

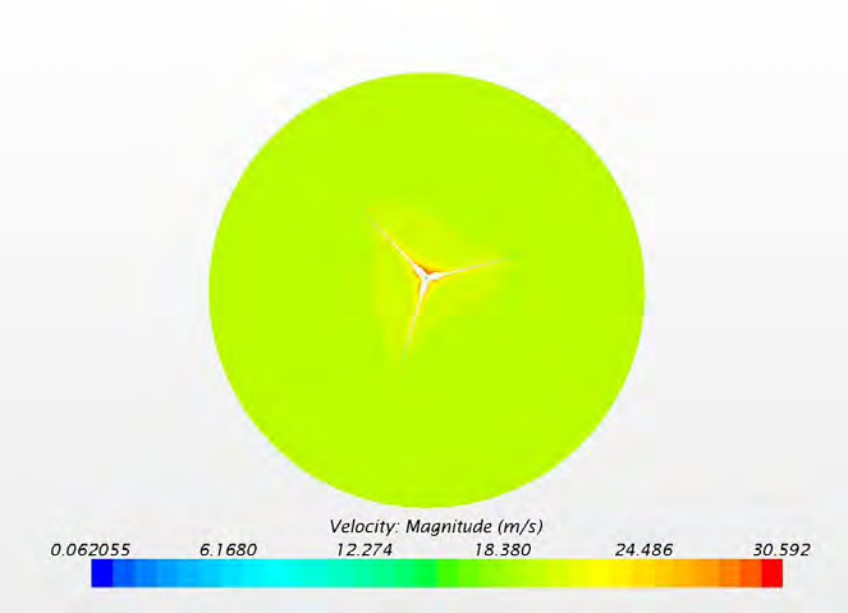

Figure 1: Velocity contour of the turbine plane from the DFBI study with a free stream velocity of 20.0 m/s.

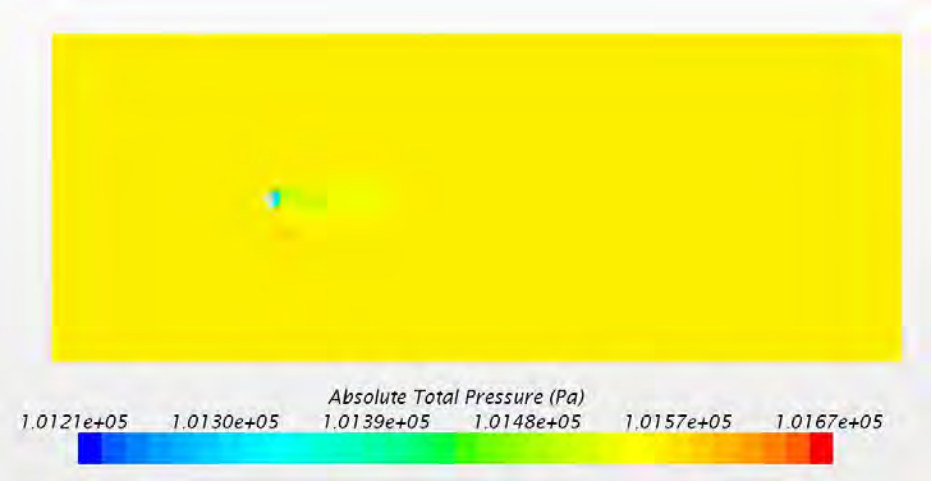

Figure 2: Pressure contour of the wake from the DFBI study with a free stream velocity of 20.0 m/s.

Appendix 3: Additional images from Actuator Disk Model study using Spalart-Allmaras turbulence model

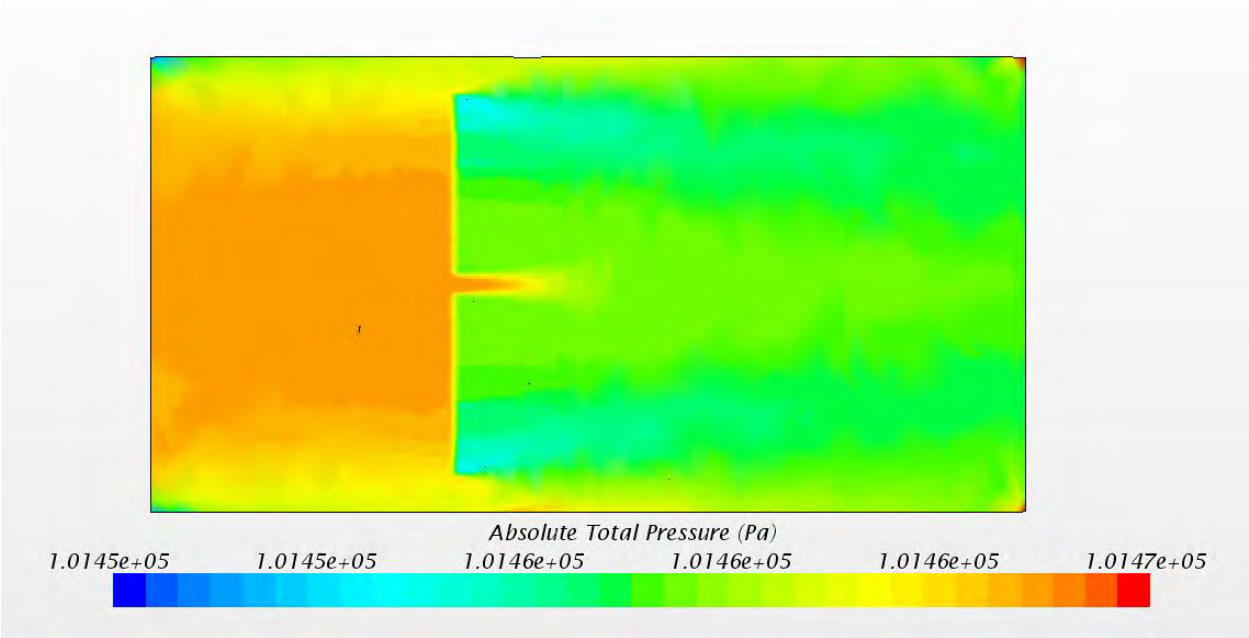

Figure 1: Pressure contour for the actuator disk model with a free stream velocity of 15.0m/s.

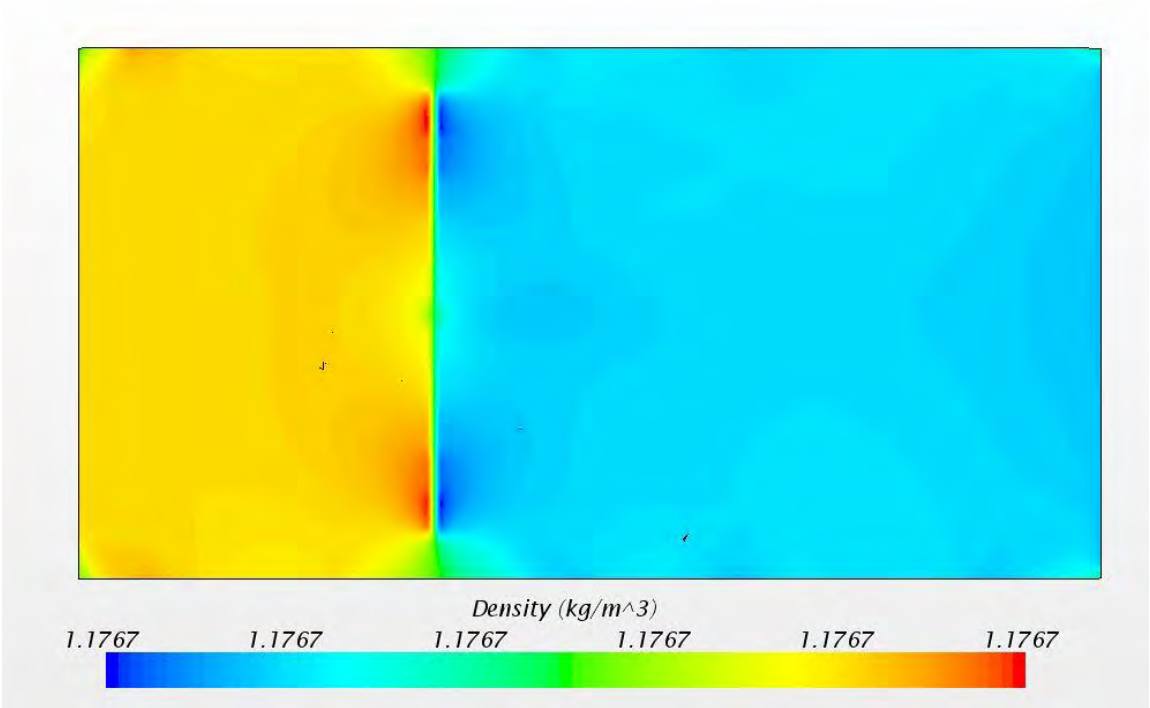

Figure 2: Density contour plot from the spalart-allmaras actuator disk model with a free stream velocity of 7.0m/s.